Monthly Notices
of the
ROYAL ASTRONOMICAL SOCIETY

MNRAS **447,** 2322–2347 (2015) doi:10.1093/mnras/stu2525

Spatial distribution of Galactic Wolf–Rayet stars and implications for the global population

C. K. Rosslowe★ and P. A. Crowther

Department of Physics and Astronomy, University of Sheffield, Hicks Building, Hounsfield Road, S3 7RH, UK

Accepted 2014 November 26. Received 2014 November 26; in original form 2014 September 5

ABSTRACT

We construct revised near-infrared absolute magnitude calibrations for 126 Galactic Wolf–Rayet (WR) stars at known distances, based in part upon recent large-scale spectroscopic surveys. Application to 246 WR stars located in the field permits us to map their Galactic distribution. As anticipated, WR stars generally lie in the thin disc (∼40 pc half-width at half-maximum) between Galactocentric radii 3.5–10 kpc, in accordance with other star formation tracers. We highlight 12 WR stars located at vertical distances of ≥300 pc from the mid-plane. Analysis of the radial variation in WR subtypes exposes a ubiquitously higher $N_{\rm WC}/N_{\rm WN}$ ratio than predicted by stellar evolutionary models accounting for stellar rotation. Models for non-rotating stars or accounting for close binary evolution are more consistent with observations. We consolidate information acquired about the known WR content of the Milky Way to build a simple model of the complete population. We derive observable quantities over a range of wavelengths, allowing us to estimate a total number of 1900 ± 250 Galactic WR stars, implying an average duration of ∼0.4 Myr for the WR phase at the current Milky Way star formation rate. Of relevance to future spectroscopic surveys, we use this model WR population to predict follow-up spectroscopy to $K_S \simeq 17.5$ mag will be necessary to identify 95 per cent of Galactic WR stars. We anticipate that ESA's *Gaia* mission will make few additional WR star discoveries via low-resolution spectroscopy, though will significantly refine existing distance determinations. Appendix A provides a complete inventory of 322 Galactic WR stars discovered since the VIIth catalogue (313 including Annex), including a revised nomenclature scheme.

Key words: stars: distances – stars: evolution – stars: massive – stars: Wolf–Rayet – Galaxy: disc – infrared: stars.

1 INTRODUCTION

Massive stars exert a major influence on their immediate surroundings, and play a dominant role in the evolution of their host galaxies. Wolf–Rayet (WR) stars represent the ultimate, short-lived (< 1Myr) evolutionary phase of only the most massive ($M_i > 25\,{\rm M}_\odot$) O stars (see Crowther 2007). They possess dense and fast stellar winds, giving them characteristic strong and broad emission line spectra. Their distinctive spectral appearance befits them as effective tracers of high-mass star formation both in the Galaxy (e.g. Kurtev et al. 2007; Davies et al. 2012a) and at extragalactic distances (Schaerer & Vacca 1998). Through their powerful winds and likely fate as Type Ib/c supernovae (SNe), they are important sources of nuclear processed material to the interstellar medium (Esteban & Peimbert 1995; Dray et al. 2003), and are capable of influencing further episodes of star formation on local (Shetty & Ostriker 2008; Kendrew et al. 2012) and galactic (Hopkins, Quataert & Murray 2011) scales. However, the postulated link between WR stars and H-free Type Ib/c SN remains unestablished (Eldridge et al. 2013), hence it is crucial that we better our knowledge of the uniquely resolvable population in the Milky Way.

Strong mass-loss in WR stars proceeds to unveil successive layers of nuclear processed material, such that examples are seen with spectra dominated by nitrogen (WN), carbon (WC), and oxygen (WO). WC and WO stars are universally H free and He rich, whereas the surface H mass fraction of WN stars varies from zero to $X_{\rm H} \simeq 50$ per cent. A subset of H-rich WN stars display weak hydrogen emission and *intrinsic* hydrogen absorption lines, referred to here as WNha stars (see Crowther & Walborn 2011). These stars are almost uniquely found in young clusters, suggesting current masses >65 $\,{\rm M}_\odot$ from cluster turn-offs and higher luminosities than their core He-burning counterparts (Crowther et al. 1995a), and hence are very rare. They differ from 'classical' He core-burning WR stars in that they represent an extension of the upper main sequence (MS), and are thought to be H burning. We treat these

*E-mail: chris.rosslowe@sheffield.ac.uk

objects separately from other WN stars when calibrating absolute magnitudes.

Our knowledge of the Galaxy's WR content rests on the successive achievements of tailored imaging surveys. The use of narrow-band selection techniques was pioneered by Massey & Conti (1983) and Moffat & Shara (1983) to identify extragalactic WR stars, taking advantage of strong WR star emission lines at optical wavelengths. Shara et al. (1991, 1999) applied similar methods to push the extent of the known Galactic population beyond 5 kpc from the Sun, and extension to near-infrared (IR) wavelengths has facilitated yet deeper investigation of the Galactic disc (Shara et al. 2009, 2012). Another distinctive feature of WR stars – the near-IR excess caused by free–free emission in their winds – has been exploited to yield further discoveries (Homeier et al. 2003; Hadfield et al. 2007; Mauerhan, Van Dyk & Morris 2011). These efforts, alongside several serendipitous discoveries (e.g. Clark et al. 2005; Mauerhan et al. 2010a), have brought the recognized Galactic WR star population to ∼635 as of 2014 March.[1]

Several attempts have been made to determine the total number of WR stars in the Galaxy. Maeder & Lequeux (1982) used the then-known 157 WR stars to arrive at a total of ∼1200 by assuming the surface density of WR stars to vary with Galactocentric radius ($R_{\rm G}$) in the same way as giant H II regions, including a dearth at $R_{\rm G} \lesssim 3$ kpc. To emphasize the need for IR investigation, Shara et al. (1999) created a model WR star population featuring a stellar disc of exponentially increasing density towards $R_{\rm G} = 0$. From this they inferred a total of 2500 Galactic WR stars, or 1500 if few WR stars inhabit the region $R_{\rm G} \lesssim 3$ kpc, as the decline in gas density suggests (barring the inner 500 pc). van der Hucht (2001) arrived at a much higher 6500 WR stars by extrapolating the surface density of local WR stars ($7 < R_{\rm G} < 12$ kpc) across the entire disc, neglecting the decrease in star formation rate (SFR) interior to $R_{\rm G} \sim 3$ kpc. Most recently, in the light of numerous WR star discoveries in IR surveys, Shara et al. (2009) presented an updated population model – still featuring an exponential disc of stars – yielding a total of 6400. The same work also suggested that observations of WR stars as faint as $K \simeq 15.5$ mag are necessary to achieve a completeness of 95 per cent.

The Galaxy provides a range of environments over which to test various predictions of massive star evolution, which has long been expected to depend on metallicity (Z). As the winds of hot stars are driven by the transfer of photon momentum to metal lines (see Puls, Vink & Najarro 2008 for a recent review), and mass-loss dominates the evolutionary fate of the most massive stars, we expect to observe differences between the population of evolved massive stars in the metal-rich Galactic Centre (GC) regions, and that of the metal-poor outer Galaxy. Smith (1968) first observationally demonstrated evidence for differences in WR populations between the Milky Way and Magellanic Clouds. Crowther et al. (2002) showed that WC subtype variations are primarily a consequence of denser stellar winds at higher metallicity, while WN stars have long been known to be a more heterogeneous group. Increased mass-loss is predicted to have two main effects of WR surface properties; more efficient removal of outer (hydrogen-rich) layers will lead to quicker progression through post-MS evolutionary phases, i.e. from WN to WC stages, and the accelerated spin-down of a star due to loss of angular momentum will inhibit various internal mixing processes, with implications for the lifetimes of evolutionary phases (Maeder & Meynet 2000). Systematic testing of such predictions requires statistically significant, unbiased samples of evolved massive stars, currently only available through IR investigation of the Galactic disc.

An improved set of IR tools is necessary to reveal and characterize the full Galactic WR population, allowing accurate distances and classifications to be obtained. In Section 2, we introduce improved near-IR absolute magnitude–spectral type calibrations for WR stars. In Section 3, these calibrations are applied to estimate distances to the majority of the known WR population, from which the radial variation of WR subtypes is obtained, allowing a comparison with evolutionary model predictions. In Section 4, we develop a toy model to estimate the global WR population of the Milky Way. Finally, we make predictions about the detectability of WR stars, which may be of interest to those planning future surveys. Our findings are summarized in Section 5. Appendix A lists all 322 Galactic WR stars discovered since the VIIth catalogue of van der Hucht (2001) and its Annex (van der Hucht 2006).

2 CALIBRATION OF IR ABSOLUTE MAGNITUDES FOR WR STARS

van der Hucht (2001) reviewed and updated the v-band absolute magnitude for Galactic WR stars. However, the accuracy and usefulness of this relation is limited by the relatively small number of WR stars observable at optical wavelengths. Recent discoveries of visibly obscured WR stars provide a much larger sample, from which broad-band calibrations in the near-IR may be obtained. In this section, we present a calibration of absolute magnitudes over the wavelength range 1-8 μm for each WR spectral type, extending earlier results by Crowther et al. (2006a) via additional WR stars located within star clusters that have been identified within the past decade.

2.1 Calibration sample

Adopted distances and spectral types for the WR stars used for our IR absolute magnitude calibration are shown in Tables 1–3 for WC/WO stars, WN stars, and WR stars in binary systems with OB companions, respectively. This sample is drawn from an updated online catalogue of Galactic WR stars[1] and totals 126, with 91 inhabiting clusters, 26 in OB associations and nine appearing 'isolated'. By subtype, 85 of these are nitrogen (WN) type, 40 carbon (WC) type, and 1 oxygen (WO) type. For OB associations that have been historically well studied at optical wavelengths, membership is taken from Lundström & Stenholm (1984). For WR stars in visually obscured clusters we generally accept the membership conclusions of the discovering author(s), except where noted.

For most star clusters and associations considered, there is typically more than one distance measurement to be found in the literature. Where these measurements are in general agreement we favour methods of OB-star spectrophotometry over MS fitting. A small number of WR stars, in relative isolation, have kinematic distances derived from velocity measurements of an associated nebula; we accept these distances but remain wary of kinematic distance estimates in general because of their sensitivity to the assumed Galactic rotation curve.

Where multiple consistent distance estimates are found in the literature we take an average of the reported distances – weighted by the square of the inverse uncertainty reported on each (e.g. Westerlund 1 and Car OB1) – indicated by multiple references in Tables 1–3. Cases in which inconsistent distances have been reported in the literature are discussed further in Appendix B.

[1] http://pacrowther.staff.shef.ac.uk/WRcat/

Table 1. Apparently single dust-free WO and WC stars, and dust-producing WC stars of known distance used to calibrate near-IR absolute magnitudes by spectral type. New nomenclature is explained in Appendix A.

Spectral type	WR#	Cluster	Association	Distance (kpc)	Ref.	J	H	K_S	Ref.	$A^J_{K_S}$	$A^H_{K_S}$	$\bar{A}_{K_S}$	M_{K_S}
WO2	142	Berkeley 87		1.23 ± 0.04	1	9.54	8.89	8.60	a, a, a	0.40	0.41	0.41 ± 0.01	-2.26 ± 0.07
WC4	144		Cyg OB2	1.40 ± 0.08	2	9.41	8.59	7.71	a, a, a	0.51	0.43	0.48 ± 0.02	-3.50 ± 0.13
WC5	111		Sgr OB1	1.9 ± 0.2	3, 4	7.28	7.14	6.51	a, a, a	0.07	0.07	0.07 ± 0.01	-4.95 ± 0.23
	114		Ser OB1	2.05 ± 0.09	5, 6	8.98	8.43	7.61	a, a, a	0.36	0.34	0.35 ± 0.02	-4.30 ± 0.10
WC6	23		Car OB1	2.6 ± 0.2	7, 8	7.89	7.60	7.06	a, a, a	0.10	–	0.10 ± 0.03	-5.12 ± 0.17
	*48−4	Danks 1		4.16 ± 0.60	9	13.16	11.82	10.78	a, a, a	0.84	0.65	0.75 ± 0.03	-3.06 ± 0.32
	154		Cep OB1	3.5 ± 1.0	10	9.30	9.01	8.29	a, a, a	0.19	0.20	0.19 ± 0.01	-4.62 ± 0.62
WC7	14		Anon Vel a	2.0 ± 0.1	11	7.49	7.25	6.61	a, a, a	0.12	0.07	0.11 ± 0.01	-5.00 ± 0.11
	68		Cir OB1	3.6 ± 0.3	12	9.90	9.39	8.75	a, a, a	0.25	0.08	0.20 ± 0.02	-4.23 ± 0.18
WC8	48−3	(G305.4+0.1)/Danks 1		4.16 ± 0.60	9	10.75	9.57	8.77	a, a, a	0.74	0.59	0.67 ± 0.03	-4.99 ± 0.32
	48−2	Danks 2		4.16 ± 0.60	9	10.83	9.83	8.98	a, a, a	0.67	0.66	0.67 ± 0.03	-4.78 ± 0.32
	77g	Westerlund 1		4.0 ± 0.2	13, 14	11.81	10.40	9.53	b, b, b	0.88	0.69	0.81 ± 0.04	-4.29 ± 0.13
	102k	Quintuplet		8.00 ± 0.25	15, 16	16.71	13.45	11.19	d, d, a	2.49	2.55	2.50 ± 0.08	-5.83 ± 0.12
	*124−1	Glimpse 20		4.45 ± 0.65	17	–	10.38	9.19	a, a	–	1.14	1.14 ± 0.10	-5.20 ± 0.33
	135		Cyg OB3	1.9 ± 0.2	18	7.23	7.11	6.66	a, a, a	0.07	0.10	0.08 ± 0.01	-4.81 ± 0.23
WC9	77p	Westerlund 1		4.0 ± 0.2	13, 14	10.12	9.09	8.29	b, b, b	0.76	0.76	0.76 ± 0.05	-5.48 ± 0.16
	101f	GC		8.00 ± 0.25	15, 16	18.78	15.43	13.11	e, e, e	2.65	2.78	2.72 ± 0.04	-4.12 ± 0.08
	101oa	GC		8.00 ± 0.25	15, 16	18.48	15.43	13.01	e, e, e	2.56	2.92	2.72 ± 0.04	-4.23 ± 0.08
	102h	Quintuplet		8.00 ± 0.25	15, 16	16.62	13.51	11.34	d, d, a	2.47	2.58	2.50 ± 0.08	-5.68 ± 0.12
WC8d	53			4.00 ± 1.00	19	8.75	7.92	6.84	a, a, a	–	–	0.29 ± 0.09‡	-6.43 ± 0.55
	102e	Quintuplet		8.00 ± 0.25	15, 16	17.5	13.3	10.4	d, d, d	–	–	3.1 ± 0.5†	-7.22 ± 0.51
	102f	Quintuplet		8.00 ± 0.25	15, 16	–	–	10.4	c	–	–	3.1 ± 0.5†	-7.22 ± 0.51
	113			2.0 ± 0.2	20	7.02	6.28	5.49	a, a, a	–	–	0.38 ± 0.01‡	-6.37 ± 0.22
WC9d	65		Cir OB1	3.6 ± 0.3	12	8.46	7.28	6.17	a, a, a	–	–	0.91 ± 0.04‡	-7.45 ± 0.19
	77aa	Westerlund 1		4.00 ± 0.25	13, 14	10.04	8.21	6.72	b, b, b	–	–	1.01 ± 0.14†	-7.30 ± 0.20
	77b	Westerlund 1		4.00 ± 0.25	13, 14	9.69	7.84	6.41	b, b, b	–	–	1.01 ± 0.14†	-7.61 ± 0.20
	77i	Westerlund 1		4.00 ± 0.25	13, 14	10.13	7.64	6.90	b, b, b	–	–	1.01 ± 0.14†	-7.12 ± 0.22
	77l	Westerlund 1		4.00 ± 0.25	13, 14	10.31	8.56	7.38	b, b, b	–	–	1.01 ± 0.14†	-6.64 ± 0.20
	77m	Westerlund 1		4.00 ± 0.25	13, 14	11.26	9.51	8.23	b, b, b	–	–	1.01 ± 0.14†	-5.79 ± 0.20
	77n	Westerlund 1		4.00 ± 0.25	13, 14	9.85	7.97	7.28	b, b, b	–	–	1.01 ± 0.14†	-6.74 ± 0.20
	95	Trumpler 27		2.5 ± 0.5	21	8.29	6.67	5.27	a, a, a	–	–	$0.66 \pm 0.03^{\dagger b}$	-7.38 ± 0.44
	101ea	GC		8.00 ± 0.25	15, 16	17.79	13.46	10.50	f, f, f	–	–	$3.2 \pm 0.2^{\dagger b}$	-7.22 ± 0.22
	102−2	Quintuplet		8.00 ± 0.25	15, 16	–	–	10.30	c	–	–	3.1 ± 0.5†	-7.32 ± 0.51
	102−3	Quintuplet		8.00 ± 0.25	15, 16	15.49	11.71	9.32	d, d, d	–	–	3.1 ± 0.5†	-8.30 ± 0.51
	104			2.6 ± 0.7	4	6.67	4.34	2.42	a, a, a	–	–	0.86 ± 0.02‡	-10.44 ± 0.64
	111a	SGR 1806−20		8.70 ± 1.65	22	–	13.76	11.60	g, g	–	–	$3.0 \pm 0.3^{\dagger b}$	-6.10 ± 0.51
	118−1	Quartet		6.3 ± 0.2	17	13.22	10.14	8.09	a, a, a	–	–	$1.6 \pm 0.4^{\dagger b}$	-7.51 ± 0.41

*Indicates updated spectral types based on an improved near-IR classification scheme.

Distance references: (1) Turner et al. (2006), (2) Rygl et al. (2012), (3) Mel'Nik & Dambis (2009), (4) Tuthill et al. (2008), (5) Hillenbrand et al. (1993), (6) Djurašević et al. (2001), (7) Smith (2006), (8) Hur, Sung & Bessell (2012), (9) Davies et al. (2012b), (10) Cappa et al. (2010), (11) Lundström & Stenholm (1984), (12) Vazquez et al. (1995), (13) Kothes & Dougherty (2007), (14) Koumpia & Bonanos (2012), (15) Reid et al. (2009), (16) Gillessen et al. (2013), (17) Messineo et al. (2009), (18) Reid et al. (2011), (19) Martín, Cappa & Testori (2007), (20) Esteban & Rosado (1995), (21) Crowther et al. (2006a), and (22) Bibby et al. (2008).

Photometry references: (a) 2MASS, (b) Crowther et al. (2006a), (c) Liermann, Hamann & Oskinova (2009), (d) Figer, McLean & Morris (1999), (e) Dong, Wang & Morris (2012), (f) Eikenberry et al. (2004), and (g) Bibby et al. (2008).

Extinction: †Average of parent cluster, ‡A_v taken from van der Hucht (2001) and converted using $A_K = 0.12A_v$.

2.2 Classification of WR stars from near-infrared spectra

Spectral types of approximately 50 per cent of our calibration sample have been obtained from optical spectroscopy following Smith, Shara & Moffat (1996) for WN subtypes and Crowther, De Marco & Barlow (1998) for WC and WO subtypes. For the remaining objects, we reassess published spectral types based upon their near-IR (1−5 μm) spectra, using an updated version of the scheme from Crowther et al. (2006a). Updated spectral types are shown in Tables 1–3. Diagnostics involve emission line equivalent width ratios drawn from adjacent ionization stages of the same atomic species. Full details will be presented elsewhere, but we shall briefly discuss the methodology here.

2.2.1 *WN diagnostics*

For WN stars, ratios of He II/He I lines provide the primary classification diagnostics; particularly He II 1.012 μm/He I 1.083 μm in the J band and He II+Brγ 2.165 μm/He II 2.189 μm in the K band. Degeneracies in these primary line ratios between spectral types are lifted by considering various weaker lines. For example, we find WN7–9 types can be distinguished by considering the strength of Si IV 1.190 μm relative to He II 1.163 μm, while an inspection of spectral morphology in the K band permits WN4–6 stars to be distinguished using N V 2.100 μm and N III 2.116 μm.

2.2.2 *WC diagnostics*

For WC stars, ratios of C II–IV provide the primary classification diagnostics, with C IV 1.191 μm/C III 0.972 μm in the J band permitting a consistent classification to optical lines. He II 1.012 μm/He I 1.083 μm also prove useful for classification, although the H band contains little diagnostic information. However, we find the very strong C IV 1.736 μm line to be useful for recognizing the dilution effects of hot circumstellar dust (see Section 2.3.2). In the K

Table 2. Apparently single WN stars (and those with an insignificant companion contribution at IR wavelengths) of known distance used to calibrate near-IR absolute magnitudes by spectral type. New nomenclature is explained in Appendix A.

Spectal type	WR#	Cluster	Association	Distance (kpc)	Ref.	J	H	K_S	Ref.	$A^J_{K_S}$	$A^H_{K_S}$	$\bar{A}_{K_S}$	M_{K_S}
WN2b	2		Cas OB1	2.4 ± 0.8	23	10.04	9.78	9.45	a, a, a	0.33	0.52	0.40 ± 0.02	−2.86 ± 0.72
WN3b	46		Cru OB4	4.00 ± 0.85	24, 25	10.20	10.08	9.83	a, a, a	0.23	0.39	0.27 ± 0.01	−3.45 ± 0.46
WN4b	1		Cas OB7	2.3 ± 0.5	3	8.21	7.86	7.48	a, a, a	0.17	0.15	0.17 ± 0.01	−4.49 ± 0.47
	6			1.80 ± 0.27	26	6.35	6.23	5.89	a, a, a	0.04	0.09	0.05 ± 0.01	−5.44 ± 0.33
	7			5.5 ± 0.5	27	9.97	9.67	9.27	a, a, a	0.16	0.19	0.17 ± 0.01	−4.60 ± 0.20
	18		Car OB1	2.6 ± 0.2	7, 8	8.57	8.21	7.68	a, a, a	0.25	0.36	0.27 ± 0.02	−4.67 ± 0.17
	35b	Sher 1		10.0 ± 1.4	28	10.95	10.35	9.76	a, a, a	0.39	0.46	0.41 ± 0.03	−5.65 ± 0.31
WN6b	*102c	Quintuplet		8.00 ± 0.25	15, 16	–	13.12	11.53	d, d	–	1.78	1.78 ± 0.38	−4.77 ± 0.44
	111c	SGR 1806-20		8.70 ± 1.65	22	–	14.03	12.16	f, f	–	2.25	2.25 ± 0.15	−4.79 ± 0.44
	134		Cyg OB3	1.9 ± 0.2	18	6.72	6.52	6.13	a, a, a	0.10	0.17	0.12 ± 0.01	−5.39 ± 0.23
	136		Cyg OB1	1.3 ± 0.2	29	6.13	5.90	5.56	a, a, a	0.09	0.10	0.09 ± 0.01	−5.10 ± 0.33
WN7b	77sc	Westerlund 1		4.0 ± 0.2	13, 14	10.34	9.11	8.37	b, b, b	0.76	0.66	0.74 ± 0.05	−5.38 ± 0.16
	111−2	Cl 1813−178		3.6 ± 0.7	30	9.62	8.60	7.94	a, a, a	0.62	0.55	0.59 ± 0.03	−5.44 ± 0.42
WN3	152		Cep OB1	3.5 ± 1.0	10	10.49	10.32	10.04	a, a, a	0.26	0.43	0.31 ± 0.02	−2.99 ± 0.62
WN5	77e	Westerlund 1		4.0 ± 0.2	13, 14	11.70	10.30	9.70	b, b, b	0.87	0.62	0.79 ± 0.06	−4.10 ± 0.16
	77q	Westerlund 1		4.0 ± 0.2	13, 14	11.92	10.84	10.26	b, b, b	0.70	0.59	0.67 ± 0.04	−3.42 ± 0.13
	77sd	Westerlund 1		4.0 ± 0.2	13, 14	12.36	11.08	10.25	b, b, b	0.92	0.94	0.93 ± 0.04	−3.69 ± 0.13
WN6	67	Pismis 20	Cir OB1	3.6 ± 0.3	12	9.28	8.86	8.45	a, a, a	0.31	0.35	0.32 ± 0.02	−4.65 ± 0.18
	77sb	Westerlund 1		4.0 ± 0.2	13, 14	11.00	9.98	9.45	b, b, b	0.65	0.52	0.61 ± 0.04	−4.17 ± 0.12
	77a	Westerlund 1		4.0 ± 0.2	13, 14	11.72	10.67	10.00	b, b, b	0.73	0.72	0.73 ± 0.04	−3.74 ± 0.13
	77s	Westerlund 1		4.0 ± 0.2	13, 14	10.77	9.72	9.20	b, b, b	0.66	0.51	0.61 ± 0.04	−4.42 ± 0.12
	85			2.8 ± 1.1	31	–	7.94	7.48	a, a	–	0.43	0.43 ± 0.16	−5.19 ± 0.87
	*101o	GC		8.00 ± 0.25	15, 16	17.94	14.13	11.60	e, e, e	3.00	3.20	3.11 ± 0.04	−6.02 ± 0.08
	115		Ser OB1	2.05 ± 0.09	5, 6	7.99	7.42	6.95	a, a, a	0.41	0.44	0.42 ± 0.02	−5.03 ± 0.10
WN7	75ba			4.1 ± 0.4	32	10.22	9.29	8.91	a, a, a	0.56	0.39	0.51 ± 0.04	−4.67 ± 0.23
	77r	Westerlund 1		4.0 ± 0.2	13, 14	11.63	10.31	9.61	b, b, b	0.90	0.83	0.87 ± 0.04	−4.27 ± 0.13
	77j	Westerlund 1		4.0 ± 0.2	13, 14	11.36	9.97	9.28	b, b, b	0.93	0.82	0.89 ± 0.04	−4.62 ± 0.13
	77d	Westerlund 1		4.0 ± 0.2	13, 14	11.06	9.83	9.26	b, b, b	0.80	0.65	0.74 ± 0.04	−4.49 ± 0.13
	*77sa	Westerlund 1		4.0 ± 0.2	13, 14	12.11	10.75	10.04	b, b, b	0.92	0.85	0.89 ± 0.04	−3.86 ± 0.13
	78	NGC 6231	Sco OB1	1.64 ± 0.03	33	5.44	5.27	4.98	a, a, a	0.16	0.25	0.18 ± 0.01	−6.27 ± 0.05
	87	Halven–Moffat 1		3.3 ± 0.3	34	8.00	7.45	7.09	a, a, a	0.37	0.36	0.37 ± 0.02	−5.88 ± 0.20
	*101ai	GC		8.00 ± 0.25	15, 16	–	14.33	12.12	e, e	–	2.84	2.84 ± 0.07	−5.23 ± 0.10
	*111−4	Cl 1813−178		3.6 ± 0.7	30	10.31	9.27	8.66	a, a, a	0.72	0.70	0.71 ± 0.03	−4.84 ± 0.42
WN8	12•	Bochum 7		4.2 ± 2.1	35	8.62	8.26	7.87	a, a, a	0.29	0.40	0.32 ± 0.02	−5.57 ± 1.09
	*48−7	Danks 1		4.16 ± 0.60	9	9.81	8.48	7.65	a, a, a	0.97	1.01	0.99 ± 0.04	−6.43 ± 0.32
	66		Cir OB1	3.6 ± 0.3	12	8.93	8.48	8.15	a, a, a	0.31	0.31	0.31 ± 0.02	−4.94 ± 0.18
	77c	Westerlund 1		4.0 ± 0.2	13, 14	10.89	9.57	8.86	b, b, b	0.90	0.85	0.88 ± 0.04	−5.03 ± 0.13
	77h	Westerlund 1		4.0 ± 0.2	13, 14	10.75	9.42	8.76	b, b, b	0.89	0.77	0.84 ± 0.04	−5.09 ± 0.13
	89	Halven–Moffat 2		3.3 ± 0.3	34	7.39	6.96	6.58	a, a, a	0.32	0.39	0.34 ± 0.02	−6.36 ± 0.20
	101b	GC		8.00 ± 0.25	15, 16	–	13.53	11.43	e, e	–	2.69	2.69 ± 0.06	−5.77 ± 0.09
	101nc	GC		8.00 ± 0.25	15, 16	17.38	14.23	11.91	e, e, e	2.60	2.99	2.79 ± 0.04	−5.40 ± 0.08
	*101oc	GC		8.00 ± 0.25	15, 16	18.66	14.93	12.61	e, e, e	2.89	2.99	2.94 ± 0.04	−4.85 ± 0.08
	*101dd	GC		8.00 ± 0.25	15, 16	18.96	15.43	13.01	e, e, e	2.84	3.12	2.98 ± 0.04	−4.49 ± 0.08
	102a	Arches		8.00 ± 0.25	15, 16	17.17	13.26	11.02	h, a, a	2.94	2.88	2.91 ± 0.05	−6.40 ± 0.10
	*102ae	Arches		8.00 ± 0.25	15, 16	15.43	12.40	10.62	i, i, i	2.28	2.25	2.27 ± 0.02	−6.16 ± 0.07
	*102af	Arches		8.00 ± 0.25	15, 16	15.97	12.81	10.88	i, i, i	2.42	2.46	2.44 ± 0.03	−6.08 ± 0.07
	*102ah	Arches		8.00 ± 0.25	15, 16	15.23	12.03	10.07	i, i, i	2.45	2.50	2.48 ± 0.03	−6.92 ± 0.07
	*102al	Arches		8.00 ± 0.25	15, 16	15.11	12.09	10.24	i, i, i	2.31	2.34	2.33 ± 0.02	−6.60 ± 0.07
	124			3.35 ± 0.67	36	8.58	8.18	7.73	a, a, a	0.34	0.47	0.39 ± 0.02	−5.28 ± 0.44
WN9	*48−6	(G305.4+0.1)/Danks 1		4.16 ± 0.60	9	10.21	8.57	7.58	a, a, a	1.19	1.24	1.21 ± 0.05	−6.73 ± 0.32
	*48−10	Danks 1		4.16 ± 0.60	9	9.42	8.15	7.48	a, a, a	0.86	0.79	0.83 ± 0.04	−6.45 ± 0.32
	48-9	Danks 1		4.16 ± 0.60	9	8.26	7.27	6.61	a, a, a	0.72	0.77	0.74 ± 0.03	−7.22 ± 0.32
	77k	Westerlund 1		4.0 ± 0.2	13, 14	9.08	7.72	7.19	b, b, b	0.84	0.59	0.75 ± 0.04	−6.57 ± 0.13
	*101m	GC		8.00 ± 0.25	15, 16	16.58	13.53	11.32	e, e, e	2.50	2.84	2.67 ± 0.03	−5.86 ± 0.08
	*101e	GC		8.00 ± 0.25	15, 16	15.87	12.73	10.41	e, e, e	2.60	2.99	2.79 ± 0.04	−6.90 ± 0.08
	*102aa	Arches		8.00 ± 0.25	15, 16	–	–	11.18	j	–	–	2.48 ± 0.37†	−5.82 ± 0.39
	*102ad	Arches		8.00 ± 0.25	15, 16	15.86	12.44	10.35	i, i, i	2.63	2.69	2.66 ± 0.03	−6.83 ± 0.08
	*102ag	Arches		8.00 ± 0.25	15, 16	15.67	12.45	10.46	i, i, i	2.48	2.55	2.52 ± 0.03	−6.58 ± 0.07
	*102ai	Arches		8.00 ± 0.25	15, 16	–	12.24	10.34	a, a	–	2.41	2.41 ± 0.19	−6.59 ± 0.22
	*102aj	Arches		8.00 ± 0.25	15, 16	16.55	13.56	11.79	i, i, i	2.26	2.24	2.25 ± 0.02	−4.98 ± 0.07
	*102bb	Arches		8.00 ± 0.25	15, 16	15.58	12.36	10.36	i, i, i	2.48	2.54	2.52 ± 0.03	−6.67 ± 0.07
	*102bc	Arches		8.00 ± 0.25	15, 16	–	13.14	11.20	i, i	–	2.47	2.47 ± 0.13	−5.79 ± 0.16
	102d	Quintuplet		8.00 ± 0.25	15, 16	15.58	12.40	10.50	d, d, c	2.41	2.42	2.42 ± 0.09	−6.43 ± 0.15

Table 2 – *continued*

Spectal type	WR#	Cluster	Association	Distance (kpc)	Ref.	J	H	K_S	Ref.	$A^J_{K_S}$	$A^H_{K_S}$	$\bar{A}_{K_S}$	M_{K_S}
	102hb	Quintuplet		8.00 ± 0.25	15, 16	14.19	10.90	9.60	d, d, c	2.18	1.61	2.01 ± 0.09	−6.93 ± 0.15
	102i	Quintuplet		8.00 ± 0.25	15, 16	14.77	11.67	10.22	d, a, a	2.16	1.81	1.98 ± 0.05	−6.27 ± 0.10
	102j	Quintuplet		8.00 ± 0.25	15, 16	14.66	11.77	10.23	a, a, a	2.10	1.94	2.03 ± 0.03	−6.32 ± 0.08
	105		Sgr OB1	1.9 ± 0.2	3, 4	7.04	6.25	5.73	a, a, a	0.56	0.58	0.57 ± 0.02	−6.24 ± 0.23
WN6ha	20a1			8.0 ± 1.0	37	9.61	8.84	8.34	a, a, a	0.61	0.65	0.63 ± 0.03	−6.80 ± 0.38
	20a2			8.0 ± 1.0	37	9.61	8.84	8.34	a, a, a	0.61	0.65	0.63 ± 0.03	−6.80 ± 0.38
	24	Coll 228	Car OB1	2.6 ± 0.2	7, 8	6.10	6.01	5.82	a, a, a	0.14	0.23	0.16 ± 0.01	−6.42 ± 0.17
	25•	Trumpler 16	Car OB1	2.6 ± 0.2	7, 8	6.26	5.97	5.72	a, a, a	0.26	0.31	0.28 ± 0.02	−6.63 ± 0.17
	43A1	NGC 3603		7.6 ± 0.4	38	8.57	8.36	7.78	k, k, k	0.38	0.77	0.49 ± 0.05	−7.11 ± 0.16
	43A2	NGC 3603		7.6 ± 0.4	38	8.98	8.77	8.19	k, k, k	0.38	0.77	0.49 ± 0.04	−6.70 ± 0.14
	43B	NGC 3603		7.6 ± 0.4	38	7.78	7.70	7.08	k, k, k	0.34	0.83	0.47 ± 0.03	−7.80 ± 0.13
	43C•	NGC 3603		7.6 ± 0.4	38	8.49	8.13	7.81	k, k, k	0.33	0.41	0.35 ± 0.03	−6.95 ± 0.13
WN7ha	22		Car	2.6 ± 0.2	7, 8	5.71	5.58	5.39	a, a, a	0.17	0.26	0.20 ± 0.03	−6.81 ± 0.17
	*125−3	Mercer 23		6.5 ± 0.3	39	8.65	7.84	7.33	l, l, l	0.64	0.70	0.67 ± 0.02	−7.40 ± 0.10
WN9ha	79a	NGC 6231	Sco OB1	1.64 ± 0.03	33	5.15	5.09	4.90	a, a, a	0.14	0.25	0.17 ± 0.02	−6.34 ± 0.05
	79b		KQ Sco	3.5 ± 0.5	40	6.76	6.62	6.48	a, a, a	0.16	0.19	0.17 ± 0.01	−6.41 ± 0.31

*Indicates updated spectral types based on an improved near-IR classification scheme.
Spectroscopic binary systems with a dominant WR component at IR wavelengths ($F^{WR}/F^{sys} > 2/3$). Binary detections: (WR 12) Fahed & Moffat (2012), (WR 25) Gamen et al. (2006), (WR 43C) Schnurr et al. (2008), and (WR 22) Schweickhardt et al. (1999).
Distance references (1–22 as in Table 1): (23) Arnal et al. (1999), (24) Crowther, Smith & Hillier (1995b), (25) Tovmassian, Navarro & Cardona (1996), (26) Howarth & Schmutz (1995), (27) Cappa et al. (1999), (28) Moffat, Shara & Potter (1991), (29) Garmany & Stencel (1992), (30) Messineo et al. (2011), (31) Vázquez et al. (2005), (32) Cohen, Parker & Green (2005), (33) Sana et al. (2006), (34) Vázquez & Baume (2001), (35) Corti, Bosch & Niemela (2007), (36) Marchenko, Moffat & Crowther (2010), (37) Rauw et al. (2007), (38) Melena et al. (2008), (39) Hanson et al. (2010), and (40) Bohannan & Crowther (1999).
Photometry references (a–g as in Table 1): (h) Cotera et al. (1999), (i) Espinoza, Selman & Melnick (2009), (j) Martins et al. (2008), (k) Harayama, Eisenhauer & Martins (2008), and (l) Hanson et al. (2010).
Extinction: †Average of parent cluster.

Table 3. WR stars in confirmed binary systems (WR+non-WR) used for absolute magnitude–spectral type calibrations.

WR#	Spectral type	Cluster/association	Distance (kpc)	Ref.	$J\,H\,K_S^{sys}$	Ref.	Flux ratio F^{WR}/F^{sys}	Extinction	M^{WR}
11	WC8+O7.5III		0.342 ± 0.035	41	$J = 2.12$	m	0.45 ± 0.32	0.00	$M_J = -4.68 \pm 0.81$
					$H = 2.17$	m	0.48 ± 0.30	0.00	$M_H = -4.70 \pm 0.72$
					$K_S = 1.98$	m	0.60 ± 0.23	0.00	$M_{K_S} = -5.14 \pm 0.48$
77o	WN7o+?	Westerlund 1	4.0 ± 0.2	13, 14	$J = 10.34$	b	0.59 ± 0.10	2.98 ± 0.20	$M_J = -5.08 \pm 0.26$
					$K_S = 8.37$	b	0.80 ± 0.10	0.96 ± 0.05	$M_{K_S} = -5.36 \pm 0.23$
79	WC7+O5–8V	Sco OB1	1.64 ± 0.03	33	$J = 5.96$	a	0.41 ± 0.05	0.48 ± 0.03	$M_J = -4.62 \pm 0.14$
					$K_S = 5.39$	a	0.45 ± 0.05	0.16 ± 0.01	$M_{K_S} = -4.97 \pm 0.13$
93	WC7+O7–9	Pismis 24	2.0 ± 0.2	t.w.	$K_S = 5.87$	a	0.73 ± 0.72	0.58 ± 0.03‡	$M_{K_S} = -5.88 \pm 1.10$
127	WN5+O8.5V	Vul OB2	4.41 ± 0.12	42	$J = 9.18$	a	0.58 ± 0.17	0.56 ± 0.09	$M_J = -4.00 \pm 0.65$
					$H = 9.02$	a	0.59 ± 0.13	0.31 ± 0.05	$M_H = -3.93 \pm 0.26$
					$K_S = 8.76$	a	0.67 ± 0.09	0.18 ± 0.03	$M_{K_S} = -4.21 \pm 0.16$
133	WN5+O9I	NGC 6871	2.14 ± 0.07	43	$J = 6.32$	a	0.22 ± 0.05	0.55 ± 0.05	$M_J = -3.86 \pm 0.19$
					$K_S = 6.25$	a	0.23 ± 0.05	0.18 ± 0.02	$M_{K_S} = -4.04 \pm 0.19$
137	WC7+O9	Cyg OB1	1.3 ± 0.2	29	$J = 7.00$	n	0.41 ± 0.12	0.59 ± 0.07	$M_J = -3.19 \pm 0.47$
					$K_S = 6.43$	n	0.46 ± 0.13	0.19 ± 0.02	$M_{K_S} = -3.49 \pm 0.46$
139	WN5+O6III–V	Cyg OB1	1.3 ± 0.2	29	$J = 6.70$	a	0.44 ± 0.06	0.59 ± 0.06	$M_J = -3.57 \pm 0.36$
					$K_S = 6.33$	a	0.50 ± 0.07	0.19 ± 0.02	$M_{K_S} = -3.69 \pm 0.36$
141	WN5+O5III–V	Cyg OB1	1.3 ± 0.2	29	$J = 7.34$	a	0.65 ± 0.07	0.45 ± 0.15†	$M_J = -3.21 \pm 0.34$
157	WN5+?	Markarian 50	3.46 ± 0.35	44	$J = 8.22$	a	0.47 ± 0.10	0.90 ± 0.15	$M_J = -4.53 \pm 0.30$
					$K_S = 7.73$	a	0.68 ± 0.10	0.29 ± 0.04	$M_{K_S} = -4.88 \pm 0.36$

Distance references (1–40 as in Tables 1 and 2): (41) van Leeuwen (2007), (42) Turner (1980), (43) Malchenko & Tarasov (2009), (44) Baume, Vázquez & Carraro (2004), (t.w.) this work (Appendix B).
Photometry references (a–l as in Tables 1 and 2): (m) Williams et al. (1990b), (n) Williams et al. (2001).
Spectral types: (WR 11) De Marco & Schmutz (1999), (WR 77o) Crowther et al. (2006a), (WR 79) Smith, Shara & Moffat (1990), (WR 93) Lortet, Testor & Niemela (1984), (WR 127) de La Chevrotière, Moffat & Chené (2011), (WR 133) Underhill & Hill (1994), (WR 137) Williams et al. (2001), (WR 139) Marchenko, Moffat & Koenigsberger (1994), (WR 141) Marchenko, Moffat & Eenens (1998), and (WR 157) Smith et al. (1996).
Extinction: ‡A_v taken from van der Hucht (2001) and converted using $A_K = 0.12A_v$. †Average extinction taken from WR 136 and WR 139, also members of Cyg OB1.

band, the ratio of C IV 2.070-2.084 μm to C III+He I 2.112-2.114 μm serves as a good ionization diagnostic, but is incapable of discriminating between WC4–6 stars.

2.2.3 *Accuracy of near-IR spectral types*

To gain an insight into the reliability of our revised near-IR classification scheme, we have carried out blind tests using WR stars with optically derived spectral types, and find *J*- and *K*-band diagnostics provide the highest level of consistency.

For WN stars, an exact 3D spectral type (Smith et al. 1996) can be achieved from low-resolution *J* through *K* spectra, with solely the *J* band proving criteria for identifying the presence of hydrogen. We find spectra in *J* or K alone yield spectral types with an accuracy of ± 1, and *H*-band diagnostics are accurate to ± 2.

For WC stars, we find that an exact spectral type can be assigned solely from a *J*-band spectrum. Our *K*-band diagnostics are capable of ± 1 spectral type amongst early (WC4–6) types, and exact classification for late (WC7–9). We only find it possible to distinguish between WCE/WCL using spectra from *H*, *L* or *M* bands. For both WN and WC stars, ionization types at either extreme (WN9, 3, 2; WC9) are conspicuous in spectral appearance, and can be identified with a higher degree of certainty, usually by inspection of the spectral morphology alone. Stars are only included in our calibration sample if we are confident within ± 1 of their spectral types.

2.3 Photometry and extinction

In general we take JHK_S photometry for each WR star from the Two Micron All-Sky Survey (2MASS) point source catalogue (Skrutskie et al. 2006), plus [3.6]-[8.0](μm) photometry from the GLIMPSE survey (Benjamin et al. 2003) for sufficiently isolated sources in the surveyed field.

We require a minimum quality flag of C where 2MASS photometry is used. Many cluster and association members are located in fields too crowded for 2MASS to be useful. In such cases, we turn to dedicated observations with higher spatial resolution of the stellar groupings in question (Tables 1–3).

We have attempted to ensure consistency in the near-IR photometry used. For example, observations of WR stars in the GC region are assembled by Dong et al. (2012), consisting of *Hubble Space Telescope* snapshot imaging plus multiple ground-based observations. In this case, to maintain consistency with other assembled photometry, we construct and apply a simple algorithm to convert the Dong et al. JHK_S values into the 2MASS photometric system (following their equations 7–9). However, in general we regard the slight differences between ground-based filter systems as insignificant, as they have a much smaller effect on calculated absolute magnitudes than that of distance uncertainties.

We calculate an extinction towards each calibration star by evaluating the colour excesses E_{J-K_S} and E_{H-K_S}, utilizing intrinsic JHK_S WR colours given by Crowther et al. (2006a), updated in Table 4. Two values of K_S-band extinction follow:

$$A^J_{K_s} = E_{J-K_s} \times \left(\frac{A_J}{A_{K_S}} - 1 \right)^{-1} \quad (1)$$

and

$$A^H_{K_s} = E_{H-K_s} \times \left(\frac{A_H}{A_{K_S}} - 1 \right)^{-1}. \quad (2)$$

The second terms in equations (1) and (2) require knowledge of the near-IR extinction law.

Table 4. Intrinsic colours adopted for each type of WR star, primarily from Crowther et al. (2006a), supplemented with unpublished stellar atmospheric model results for additional types considered here (e.g. WO).

Spectral type	$(J-K_S)_0$	$(H-K_S)_0$
WO2	0.11	0.00
WC4–7	0.62	0.58
WC8	0.43	0.38
WC9	0.23	0.26
WN4–7b	0.37	0.27
WN2–4	− 0.11	− 0.03
WN5–6	0.18	0.16
WN7–9	0.13	0.11
WN5–6ha	− 0.015	0.03
WN7–9ha	− 0.04	0.005

Due to the growing body of evidence suggesting a difference in dust properties towards the GC, we employ two different Galactic near-IR extinction laws. For stars in the GC region ($358^\circ < l < 2^\circ$, $|b| < 1^\circ$) we use the line-derived extinction law of Fritz et al. (2011) ($A_J/A_{K_S} = 3.05 \pm 0.07$, $A_H/A_{K_S} = 1.74 \pm 0.03$). For all other Galactic sight lines we use the law of Stead & Hoare (2009) ($A_J/A_{K_S} = 3.1 \pm 0.2$, $A_H/A_{K_S} = 1.71 \pm 0.09$) – an updated form of that provided by Indebetouw et al. (2005). For the purpose of calculating the absolute magnitude of each calibration star, we take an average, $\bar{A}_{K_S}$, from equations (1) and (2). Since extinction in the IRAC bands is lower, we opt for a more straightforward approach and use the relations given by Indebetouw et al. (2005), independent of sight line.

A minority of stars in our calibration sample only have single-band photometry available, preventing an extinction calculation by colour excess. For these objects, we resort to one of two alternatives; we adopt the average A_{K_S} calculated for other O or WR stars in the cluster/association if sufficient numbers are available, or we take A_v as listed in van der Hucht (2001) and convert this using $A_{K_S} \simeq 0.11 A_V \simeq 0.12 A_v$ (Rieke & Lebofsky 1985). If neither is possible we exclude the star from our sample.

2.3.1 *Correction for binary companions*

For cluster/OB association WR stars in spectroscopically confirmed binary systems, we attempt to correct for the contribution of companion(s) to systemic magnitudes, allowing an absolute magnitude calculation for the WR component. Depending on the information available about the companion star(s), we follow one of two methods to apply these corrections.

If the companion is an OB star of known spectral type, we use the synthetic photometry of Martins & Plez (2006), or *Hipparcos*-based absolute magnitudes (Wegner 2006), to correct for its contribution. Otherwise we determine a WR/companion continuum flux ratio by considering dilution of the WR emission lines in the bands where line measurements are available. The *single-star* emission line strengths used to determine WR/companion continuum flux ratios are presented in Appendix C. If the companion is not an OB star or is insufficiently bright to notably dilute WR emission lines, it will not make a significant contribution to the combined light. 10 of the WR stars in our calibration sample, detailed in Table 3, have been corrected by one of these methods.

Table 5. Calibrated near-IR absolute magnitudes for Galactic WR stars. The number of objects used to arrive at each value is indicated in adjacent parentheses. Two uncertainties are shown with each value; formal errors (parenthesized, equation 5) do not account for the intrinsic spread in magnitude within a WR spectral type – estimated to be ∼0.3 mag – which is incorporated into the final (non-parenthesized) uncertainty.

Spectral type	$\bar{M}_J$	(*N*)	$\bar{M}_H$	(*N*)	$\bar{M}_{K_S}$	(*N*)
WO2	−2.15 ± (0.08) 0.31	(1)	−2.26 ± (0.08) 0.31	(1)	−2.26 ± (0.07) 0.31	(1)
WC4	−2.88 ± (0.13) 0.33	(1)	−2.92 ± (0.13) 0.33	(1)	−3.50 ± (0.13) 0.33	(1)
WC5	−3.80 ± (0.27) 0.40	(2)	−3.84 ± (0.27) 0.40	(2)	−4.40 ± (0.25) 0.39	(2)
WC6	−4.03 ± (0.61) 0.68	(3)	−4.06 ± (0.62) 0.69	(3)	−4.66 ± (0.61) 0.68	(3)
WC7	−4.21 ± (0.20) 0.36	(4)	−4.25 ± (0.20) 0.36	(2)	−4.84 ± (0.21) 0.36	(5)
WC8	−4.26 ± (0.24) 0.38	(6)	−4.35 ± (0.22) 0.37	(7)	−5.04 ± (0.28) 0.41	(7)
WC9	−4.42 ± (0.39) 0.49	(4)	−4.17 ± (0.32) 0.44	(4)	−4.57 ± (0.38) 0.48	(4)
WC8d	−5.53 ± (0.25) 0.39	(3)	−5.83 ± (0.23) 0.38	(3)	−6.57 ± (0.27) 0.41	(4)
WC9d	−6.34 ± 0(.25) 0.39	(12)	−6.63 ± (0.21) 0.37	(13)	−7.06 ± (0.20) 0.36	(14)
WN2b	−2.97 ± (0.73) 0.79	(1)	−2.89 ± (0.73) 0.78	(1)	−2.86 ± (0.72) 0.78	(1)
WN3b	−3.56 ± (0.46) 0.55	(1)	−3.48 ± (0.46) 0.55	(1)	−3.45 ± (0.46) 0.55	(1)
WN4b	−4.48 ± (0.23) 0.38	(5)	−4.58 ± (0.23) 0.38	(5)	−4.85 ± (0.23) 0.38	(5)
WN5b	−4.70 ± (0.16) 0.34[a]	(0)	−4.74 ± (0.16) 0.34[a]	(0)	−5.00 ± (0.16) 0.34[a]	(0)
WN6b	−4.93 ± (0.23) 0.38	(2)	−4.90 ± (0.22) 0.37	(4)	−5.16 ± (0.22) 0.37	(4)
WN7b	−5.02 ± (0.16) 0.34	(2)	−5.12 ± (0.19) 0.36	(2)	−5.38 ± (0.15) 0.34	(2)
WN3	−3.10 ± (0.62) 0.69	(1)	−3.02 ± (0.62) 0.69	(1)	−2.99 ± (0.62) 0.69	(1)
WN4	−3.36 ± (0.32) 0.44[a]	(0)	−3.33 ± (0.32) 0.44[a]	(0)	−3.39 ± (0.32) 0.44[a]	(0)
WN5	−3.63 ± (0.16) 0.34	(8)	−3.66 ± (0.15) 0.34	(4)	−3.86 ± (0.15) 0.34	(7)
WN6	−4.47 ± (0.30) 0.43	(6)	−4.74 ± (0.34) 0.45	(7)	−4.94 ± (0.34) 0.46	(7)
WN7	−5.32 ± (0.34) 0.45	(9)	−5.01 ± (0.28) 0.41	(9)	−5.49 ± (0.30) 0.42	(10)
WN8	−5.94 ± (0.19) 0.35	(15)	−5.78 ± (0.19) 0.36	(16)	−5.82 ± (0.20) 0.36	(16)
WN9	−6.18 ± (0.18) 0.35	(15)	−6.19 ± (0.16) 0.34	(17)	−6.32 ± (0.15) 0.33	(18)
WN6ha	−6.98 ± (0.17) 0.34	(8)	−6.94 ± (0.19) 0.36	(8)	−7.00 ± (0.18) 0.35	(8)
WN7ha	−7.33 ± (0.25) 0.39	(2)	−7.26 ± (0.27) 0.40	(2)	−7.24 ± (0.28) 0.41	(2)
WN9ha	−6.38 ± (0.07) 0.31	(2)	−6.33 ± (0.07) 0.31	(2)	−6.34 ± (0.05) 0.30	(2)

[a] Average of adjacent types since no stars of this type are available for calibration.

Two systems in our calibration sample are WNha+WNha binaries. There are no known 'classical' WR+WR binaries, highlighting the sensitivity of post-MS evolution to initial mass. The fact that WNha+WNha binaries *are* observed emphasizes their similarity to massive O stars. We separate the light contributions of individual stars to each system by considering mass ratios derived by spectroscopic monitoring of their orbits. The stars making up WR 20a are of identical spectral type and have very similar masses (Rauw et al. 2005), hence we assume an equal light contribution from each star in the *J, H* and K_S bands, and alter the systemic photometry accordingly. Similarly, WR 43A in the NGC 3603 cluster is comprised of two stars with very high measured masses, 116 ± 31 and 89 ± 16 $M_\odot$ ($q = 0.8 \pm 0.2$; Schnurr et al. 2008). Using the mass–luminosity relationship for very massive stars ($M > 80\,M_\odot$) provided by Yusof et al. (2013), we arrive at a light ratio of 1.46 ± 0.47 for this system in all bands, assuming identical spectral energy distributions (SEDs). We include the stars of WR 20a and WR 43A under the WN6ha spectral type in Table 2.

2.3.2 *Treatment of dust-forming WC stars*

The majority of WC9, and a diminishing fraction of earlier WC stars, show evidence of periodic or persistent circumstellar dust production (e.g. WR 140; Williams et al. 1990a). Episodes of dust formation occur at perihelion passage in eccentric WC+OB systems, whereas circular orbits allow persistent dust production, enhancing the near-IR flux of the system dramatically. For completeness, we perform near- to mid-IR absolute magnitude calibrations for WC8d and WC9d spectral types based on the 18 stars at known distances. However, we do not make any attempt to remove the light contribution of potential companion stars, firstly because their K_S-band flux is usually insignificant compared to that of the hot circumstellar dust, and secondly because dust production seems to be inextricably linked to the presence of these companions (Crowther 2003).

Thermal emission from hot circumstellar dust dominates the IR colours of dusty WC systems, prohibiting extinction determination via near-IR colour excess. For the dusty systems in our calibration sample we either adopt an average A_{K_S} for the relevant cluster/association, or its A_v from van der Hucht (2001) and convert this to the K_S band according to $A_{K_S} \simeq 0.12 A_v$.

We make an exception of WR 137 – a member of the Cyg OB1 association comprising WC7 and O9(± 0.5) type stars – which displays periodic dust formation episodes concurrent with its 13 yr orbit. Williams et al. (2001) present *JHK*$_S$ photometry for this system during a quiescent phase (1992–4), allowing us to derive a K_S-band flux ratio ($F_{\rm WR}/F_{\rm sys} = 0.46 \pm 0.13$) using line strengths measured from spectra taken during quiescence (Vacca, private communication), and remove the O-star light. The WC7 component is included in Table 3.

2.4 Calibration method and uncertainties

The results of our near-IR absolute magnitude calibrations are presented in Table 5, with mid-IR calibrations shown in Table 6. Figs 1 and 2 present the K_S-band absolute magnitudes for WN and WC stars, respectively. We use a weighted mean method to arrive at an average absolute magnitude for each WR spectral type, computed by

$$\bar{M} = \sum_{i=1}^{n} \frac{p_i M_i}{p}, \tag{3}$$

Table 6. Calibrated mid-IR (*Spitzer* IRAC filters) absolute magnitudes for Galactic WR stars. The number of objects used to arrive at each value is indicated in adjacent parentheses. Two uncertainties are shown with each value; formal errors (parenthesized, equation 5) do not account for the intrinsic spread in magnitude within a WR spectral type – estimated to be ∼0.3 mag – which is incorporated into the final (non-parenthesized) uncertainty.

WR Spectral type	$\bar{M}_{[3.6]}$	(*N*)	$\bar{M}_{[4.5]}$	(*N*)	$\bar{M}_{[5.8]}$	(*N*)	$\bar{M}_{[8.0]}$	(*N*)
WC5–6	−4.34 ± (0.35) 0.46	(2)	−4.75 ± (0.35) 0.46	(2)	−5.02 ± (0.28) 0.41	(3)	−5.32 ± (0.29) 0.41	(3)
WC7–9	−5.96 ± (0.29) 0.42	(4)	−6.27 ± (0.33) 0.45	(4)	−6.06 ± (0.33) 0.45	(4)	−6.27 ± (0.34) 0.46	(4)
WC8d	–		–		−8.18 ± (0.55) 0.63	(1)	−8.47 ± (0.55) 0.63	(1)
WC9d	−6.88 ± (0.48) 0.57	(1)	−7.25 ± (0.50) 0.58	(1)	−9.29 ± (0.16) 0.34	(4)	−9.36 ± (0.16) 0.34	(4)
WN3b	−3.59 ± (0.46) 0.55	(1)	−3.84 ± (0.46) 0.55	(1)	−4.11 ± (0.46) 0.55	(1)	−4.50 ± (0.46) 0.55	(1)
WN6–7b	−5.51 ± (0.41) 0.51	(2)	−5.88 ± (0.40) 0.50	(2)	−6.14 ± (0.38) 0.49	(2)	−6.41 ± (0.44) 0.53	(2)
WN4–6	−4.18 ± (0.13) 0.33	(1)	−4.42 ± (0.14) 0.33	(1)	−4.71 ± (0.15) 0.34	(1)	−5.05 ± (0.15) 0.33	(1)
WN7–9	−5.96 ± (0.39) 0.49	(5)	−6.23 ± (0.36) 0.47	(6)	−6.53 ± (0.28) 0.41	(12)	−6.79 ± (0.30) 0.43	(11)
WN7ha	–		−7.74 ± (0.12) 0.32	(1)	−7.87 ± (0.12) 0.32	(1)	−8.22 ± (0.12) 0.32	(1)
WN9ha	–		–		−6.79 ± (0.31) 0.43	(1)	−6.90 ± (0.31) 0.43	(1)

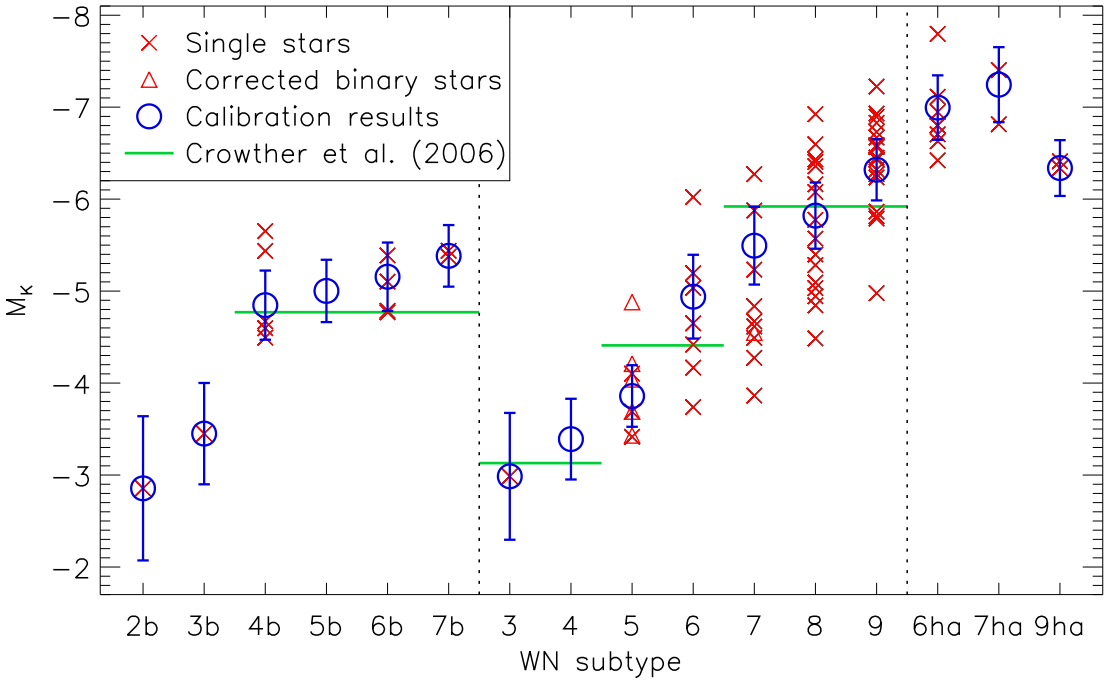

Figure 1. Calibration of M_{K_S} for WN spectral types. Broad-line stars are on the left, weak-line (including 'WN#o' and 'WN#h' stars) in the centre, and 'WN#ha' stars to the right. Individual single stars are represented by small (red) crosses, and stars that have been corrected for a companion(s) by (red) triangles. Larger (blue) symbols show the weighted average for each type with a combination of statistical error (equations 5, 6 and 7) and the estimated intrinsic spread (0.3 mag) in M_{K_S} within a WR spectral type. The horizontal lines represent the previous calibrations of Crowther et al. (2006a).

using weights

$$p_i = \frac{1}{s_i^2}, \qquad p = \sum_{i=1}^{n} p_i, \tag{4}$$

where s_i is the error in absolute magnitude (M_i) – invariably dominated by distance uncertainty – calculated for each of the n WR stars of that type. We calculate a formal error (σ) on each calibrated absolute magnitude value by combining two uncertainty estimates for weighted data:

$$\sigma = \sqrt{\sigma_1^2 + \sigma_2^2}, \tag{5}$$

where

$$\sigma_1 = \frac{1}{\sqrt{p}}, \tag{6}$$

and

$$\sigma_2 = \sqrt{\frac{\sum_{i=1}^{n} p_i (M_i - \bar{M})^2}{p(n-1)}}. \tag{7}$$

This combination is chosen because σ_1 depends only on s_i and does not consider the spread in M_i, which is taken into consideration by σ_2.

This weighted average approach favours objects with the most accurately determined distances, but the formal uncertainty given by equation (5) does not account for any *intrinsic* scatter in WR star luminosities within a spectral type. Such a scatter is expected, as a WR spectral type does not represent a perfectly uniform class of objects, but the division of smoothly varying WR properties at spectrally identifiable boundaries. Therefore, one expects each subclass to encompass a range in mass, temperature and luminosity.

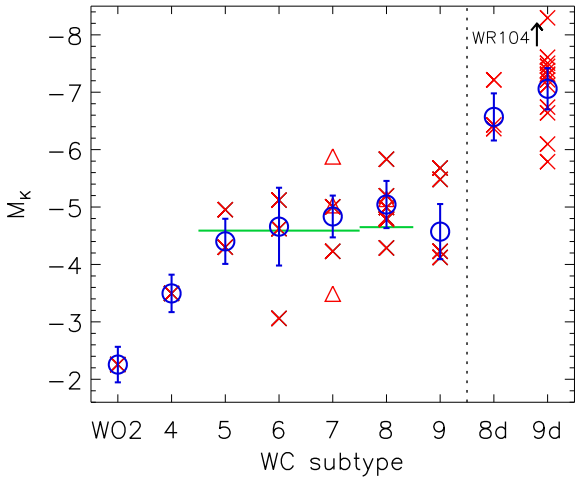

Figure 2. Calibration of M_{K_S} for WO and WC subtypes. To the right of the vertical dotted line are subtypes associated with circumstellar dust. WR 104 (WC9d+B) has $M_{K_S} = -10.4$, outside the range displayed here. Symbols same as Fig. 1.

Table 7. Intrinsic scatter in absolute magnitude within a WR spectral type.

Cluster	Stars (WR#)	M_{K_S} range	σ_{M_K}
WN7			
Westerlund 1	77d, 77j, 77r, 77sa	0.76	0.33
WN8			
Arches	102a, 102ae, 102af, 102ah, 102al	0.84	0.34
GC Cluster	101b, 101dd, 101nc, 101oc	1.28	0.57
WN9			
Arches	102ad, 102ag, 102ai, 102aj, 102bb, 102bc	1.85	0.72

Westerlund 1, the Arches and the GC cluster individually contain enough stars of a single spectral type to evaluate some basic measures of spread, effectively eliminating the scatter introduced by distance uncertainties when considering one type across multiple clusters. In Table 7, we show the range and standard deviation in M_{K_S} within a WR spectral type. Ranges are typically < 1, although WN9 stars in the Arches cluster show a larger range due to the anomalously faint WR 102aj; we classify this star based on a K-band spectrum published by Martins et al. (2008) and thus can only claim a ± 1 accuracy on the WN9 spectral type. Typical standard deviations of 0.3–0.6 mag in M_{K_S} suggest that WR absolute magnitudes intrinsically vary by at least ± 0.3 within a spectral type. Following this result, we add an uncertainty of 0.3 mag in quadrature to the result of equation (5) (see Tables 5 and 6), and recommend the adoption of this combined uncertainty when applying these calibrated absolute magnitudes to WR stars in the field.

Throughout the rest of this paper we favour discussion and application of the M_{K_S} calibration as these results are affected by lower (and more accurately determined) extinctions than those in J and H bands, and are derived using the largest sample. For completeness, in the cases of WN4 and WN5b stars (unrepresented in our calibration sample), we take average values in each band from the adjacent ionization types.

2.5 Results of near- to mid-IR absolute magnitude calibrations

Both strong- and weak-line WN stars show a monotonic increase in intrinsic near-IR brightness with ionization type. This is largely due to cooler, late-type WN stars having smaller bolometric corrections. WN stars displaying intrinsic absorption features (the 'ha' stars) are the most luminous at these wavelengths, as a consequence of their high masses. Our results show good agreement with the calibrations of Crowther et al. (2006a) for weak-line WN stars, but suggest slightly higher IR luminosities for strong-line WN4–7b. We note that for ionization types 6 and 7, strong- and weak-line stars have similar M_{K_S}. One would expect an enhanced contribution from free–free excess in the denser winds of 'b' stars to make them brighter at IR wavelengths than weak-line stars. However, the strong-line stars of these ionization types have higher effective temperatures (Hamann, Gräfener & Liermann 2006), so the enhanced IR emission from free–free excess is counteracted by larger bolometric corrections at these subtypes.

The lower number of WC stars available reveal a less obvious variation in M_{K_S} with ionization type, yet a monotonic increase in near-IR luminosity does appear to be present for WC4–8. As expected, dusty WC stars display a large range in M_{K_S} due to varying quantities of dust and the range of orbital phases sampled amongst periodic dust-forming systems.

The limited area and resolution of the GLIMPSE survey results in far fewer stars available for absolute magnitude calibration at 3.6-8.0 μm. Hence, in some cases spectral types showing only small differences in M_{K_S} are grouped together to provide more robust estimates. For all WR types with GLIMPSE coverage, we observe a brightening across [3.6]–[8.0], gradual in most cases except dusty WC stars which exhibit a dramatic $\Delta M \sim 2$ between [4.5] and [5.8], owing to hot circumstellar dust emission.

2.5.1 *The effects of a different Galactic Centre extinction law*

The results presented in this paper are produced by applying the line-derived Fritz et al. (2011) 1−19 μm law – with $A \propto \lambda^{-\alpha}$, $\alpha = 2.13 \pm 0.08$ over the JHK_S range – to WR stars residing in the GC ($358^\circ < l < 2^\circ$, $|b| < 1^\circ$). Alternatively, Nishiyama et al. (2009) propose a shallower law ($\alpha = 2.0$). It can be seen in equations (1) and (2) that a shallower law would lead to lower derived extinctions by the colour excess method. We perform a second set of absolute magnitude calibrations using the Nishiyama et al. law to quantify its effect on our results. The biggest change is seen in our calibrated absolute magnitudes for late-type WN and WC stars, as these dominate in the inner Galaxy. Compared to values presented in Table 5, adopting the Nishiyama et al. law changes $\bar{M}_J$, $\bar{M}_H$, and $\bar{M}_{K_S}$ of WN9 stars by −0.30, −0.31 and −0.30 mag, respectively; WN8 stars by −0.26, −0.31, −0.32 mag, and WC9 stars by −0.27, −0.32, −0.32 mag. All differences are within our adopted uncertainties (Table 5), and hence are not significant. However, as we proceed to obtain further results based on these values we monitor their effects and comment where discrepancies arise.

3 THE OBSERVED GALACTIC WR STAR DISTRIBUTION

The sample of WR stars involved in our absolute magnitude calibrations represents approximately 20 per cent of the current known Galactic population. The remainder either have poorly defined spectral types, uncertain binary status, or in a majority of cases do not reside in an identified cluster or association for which a distance measurement is available. For convenience, we shall refer to any WR star not in our calibration sample (i.e. Tables 1–3) as a 'field' star.

Up until recently it was widely accepted that most stars formed in clusters (Lada & Lada 2003), so the low frequency of WR stars

Table 8. Calculated spatial locations of the 228 'field' WR stars showing no conclusive evidence for an IR-bright companion, to which our calibrated absolute magnitudes have been assigned. Shown for each object are the adopted spectral type, 2MASS photometry (unless stated), derived K_S-band extinction, heliocentric distance (d), Galactocentric radius (R_G) and vertical distance from the Galactic mid-plane (z). A full version of this table is available online, and further details of stars discovered following the VIIth catalogue (WRXXX-#) are provided in Appendix A.

WR#	Spectral type	Ref.	J	H	K_S	$\bar{A}_{K_S}$	d (kpc)	R_G (kpc)	z (pc)
3	WN3ha	1	10.24	10.13	10.01	0.18 ± 0.02	4.53 ± 1.15	11.41 ± 1.18	-308 ± 83
4	WC5	2	8.75	8.57	7.88	0.13 ± 0.01	2.69 ± 0.49	10.15 ± 0.55	-121 ± 25
5	WC6	2	8.63	8.34	7.65	0.16 ± 0.02	2.69 ± 0.84	10.18 ± 0.88	-82 ± 32
13	WC6	2	10.14	9.64	8.86	0.29 ± 0.02	4.42 ± 1.38	9.46 ± 1.40	-40 ± 19
15	WC6	2	7.85	7.34	6.60	0.28 ± 0.02	1.57 ± 0.49	8.11 ± 0.55	-10 ± 9
16	WN8h	2	6.97	6.71	6.38	0.24 ± 0.02	2.77 ± 0.46	7.95 ± 0.52	-104 ± 20
17	WC5	2	9.93	9.74	9.17	0.07 ± 0.02	5.02 ± 0.91	8.31 ± 0.95	-303 ± 59
17−1	WN5b	3	11.73	10.38	9.53	0.85 ± 0.05	5.43 ± 0.86	8.58 ± 0.89	-41 ± 10
19	WC5+O9	4,5	9.75	9.13	8.53	0.20 ± 0.02	3.52 ± 0.64	7.93 ± 0.69	-54 ± 13
19a	WN7(h)	2	9.07	8.13	7.50	0.71 ± 0.04	2.41 ± 0.47	7.78 ± 0.53	-23 ± 8
...	...	...	...	...	...	...	...	...	...

Spectral types: (1) Marchenko et al. (2004), (2) van der Hucht (2001), (3) this work, (4) Crowther et al. (1998), (5) Williams, Rauw & van der Hucht (2009), ...

presently in clusters arose via dynamical ejection or rapid cluster dissolution. It is now recognized that a high fraction of star formation occurs in relatively low density regions (Bressert et al. 2010), so the low fraction of WR stars in clusters does not require an unusually high rate of ejection. Smith & Tombleson (2015) compare the association of WR stars (and luminous blue variables) in the Milky Way and Magellanic Clouds with O stars. They find WR stars to be less clustered than O-type stars, with WC stars in particular showing weak spatial coincidence with O stars and H-rich WN stars.

Our WN and WC calibration samples echo this finding, with approximately half as many WC stars residing in clusters or associations as WN stars. The typical velocity dispersion of cluster stars is not high enough to account for the isolation of WC stars considering their age. The relative isolation of WC stars challenges the commonly accepted evolutionary paradigm that this phase follows the WN phase in the lives of the most massive stars. Two alternative scenarios may explain the locations of WC stars; either they descend from a lower initial mass regime than other WR types (Sander, Hamann & Todt 2012), or the runaway fraction of WC and H-free WR stars in general is higher. Further detailed modelling of cluster collapse and the ejection of massive stars is needed to explain these emerging statistics.

In this section, we present an analysis of the spatial distribution of WR stars, where distances to 246 field WR stars are obtained by application of our absolute magnitude calibrations. Runaway WR stars are discussed further in Section 3.2.3.

3.1 Applying M_{K_S} calibrations

Photometry and the derived spatial information for 246 field WR stars are given in Tables 8 and 9. For any non-dusty field WR star with a well-defined spectral type and no evidence of a significant binary companion – either spectroscopically or through dilution of near-IR emission lines – we simply apply our M_{K_S} calibrations to obtain a distance. For these straightforward cases, we once again use 2MASS photometry and calculate extinctions by the method described in Section 2.3.

Regarding rare WO stars, although only one star (WR 142, WO2) is available for calibration, we apply the absolute magnitude of this star to the other three field WO stars in the Galaxy, spanning WO1–4 spectral types.

We find the spectral type and binary status of many field WR stars to be uncertain. The majority of the field sample are heavily reddened stars discovered by near-IR surveys, with typically only a K-band (and occasionally H-band) spectrum available in the literature; inclusion of these stars in our analysis is subject to a spectral type being attributable by our near-IR classification scheme to the required ± 1. Of the field WR stars included in this distribution analysis, we modify the previously claimed spectral types of $\sim$25 per cent of those with *only* IR data available, indicated in Tables 8 and 9. For the remaining 75 per cent, we either agree with previous spectral types based on near-IR spectra, or adopt optically assigned spectral types (always assumed to be reliable).

Further difficulty is encountered when trying to determine the binary status of each WR star, particularly late-WC stars, as IR line dilution could be a result of thermal emission from circumstellar dust *or* the continuum of a bright companion. For WR stars of types other than WC7–9 showing evidence of binarity, if a flux ratio of the WR component to its companion is determinable in either J, H or K_S, it is straightforward to adjust the corresponding 2MASS photometry to that of the WR component alone. We follow one of two procedures to obtain near-IR flux ratios for suspected binary systems, depending on whether or not the companion responsible for line dilution has been classified.

In the case of SB2 systems where both stars have been explicitly classified, we determine flux ratios in the JHK_S bands using the absolute magnitudes of Martins & Plez (2006) (O stars) or Wegner (2006) (B stars) along with our calibrated WR star absolute magnitudes. The advantage of this method is that it enables us to correct photometry over all bands, allowing an extinction calculation by our favoured colour excess method. This method is also applicable to dusty WC stars, provided photometry is available from a quiescent period.

If a (non-WC7–9) WR star shows diluted near-IR emission lines – but the nature of the diluting source is unclear – we estimate the flux ratio using single-star emission line strengths (Appendix C). The dilution of optical lines can also be used, as the uniformity of OB-star intrinsic $(V - K_S)$ colours (Martins & Plez 2006) makes it straightforward to translate a V-band flux ratio

Table 9. Calculated spatial locations of 18 binary 'field' WR stars to which our calibrated absolute magnitudes have been assigned. Shown for each object are the adopted spectral type(s), systemic 2MASS photometry (unless stated), calculated K_S-band (unless stated otherwise in parentheses) WR/system flux ratio, derived K_S-band extinction, heliocentric distance (d), Galactocentric radius (R_G) and vertical distance from the Galactic mid-plane (z).

WR#	Spectral type	Ref.	J^{sys}	H^{sys}	K_S^{sys}	F^{WR}/F^{sys}	$\bar{A}_{K_S}$	d (kpc)	R_G (kpc)	z (pc)
29	WN7h+O5I	1	9.91	9.46	9.12	0.49 ± 0.16	0.51 ± 0.19	9.48 ± 2.56	10.27 ± 2.57	-148 ± 45
30	WC6+O6–8	2	10.06	9.76	9.21	$0.75^{+0.25}_{-0.66}$	$0.25^{+0.37}_{-0.25}$	6.11 ± 3.44	8.29 ± 3.45	-258 ± 157
30a	WO4+O5–5.5	3	10.25	9.83	9.56	0.13 ± 0.04	0.40 ± 0.04	5.67 ± 1.18	8.17 ± 1.21	-117 ± 28
31	WN4+O8V	2	9.17	8.96	8.69	0.46 ± 0.23	0.30 ± 0.22	3.34 ± 1.12	7.63 ± 1.15	21 ± 1
35a	WN6h+O8.5V	4	10.47	9.98	9.65	$0.80^{+0.20}_{-0.33}$	0.37 ± 0.14	7.81 ± 1.99	9.13 ± 2.00	12 ± 2
41	WC5+OB	2	11.53	10.98	10.12	$0.93^{+0.07}_{-0.53}$	0.47 ± 0.27	6.69 ± 2.06	8.40 ± 2.07	-101 ± 37
42	WC7+O7V	5	7.59	7.52	7.08	0.53 ± 0.10(J)	0.14 ± 0.03	2.96 ± 0.53	7.47 ± 0.58	-6 ± 5
47	WN6+O5.5	6	8.32	7.92	7.55	$0.93^{+0.07}_{-0.12}$(J)	0.37 ± 0.03	2.12 ± 0.44	7.10 ± 0.50	11 ± 2
50	WC7+OB	2	9.75	9.38	8.81	$0.86^{+0.14}_{-0.59}$	$0.21^{+0.37}_{-0.21}$	5.23 ± 2.18	6.49 ± 2.19	45 ± 11
51	WN4+OB?	2	10.90	10.33	9.89	$0.77^{+0.23}_{-0.30}$	$0.72^{+0.86}_{-0.72}$	3.70 ± 1.80	6.55 ± 1.82	35 ± 7
63	WN7+OB	2	8.60	8.07	7.64	$0.89^{+0.11}_{-0.44}$	0.43 ± 0.27	3.68 ± 1.23	5.85 ± 1.26	-6 ± 8
86	WC7+B0III	7	7.44	7.14	6.67	0.77 ± 0.26	0.31 ± 0.02	1.97 ± 0.47	6.05 ± 0.53	83 ± 15
125	WC7ed+O9III	2	9.26[8]	8.74[8]	8.25[8]	0.46 ± 0.07	0.25 ± 0.12	5.45 ± 1.05	6.56 ± 1.08	120 ± 19
138	WN5+OB	2	6.97	6.80	6.58	0.61 ± 0.11	0.27 ± 0.10	1.38 ± 0.26	7.76 ± 0.36	46 ± 5
143	WC4+Be	9	8.58	8.10	7.46	0.53 ± 0.17	0.60 ± 0.06	1.33 ± 0.30	7.82 ± 0.39	18 ± 1
151	WN4+O5V	2	9.76	9.36	9.01	0.73 ± 0.10	0.40 ± 0.11	2.93 ± 0.65	9.10 ± 0.70	91 ± 16
155	WN6+O9II–Ib	2	7.48	7.34	7.16	0.70 ± 0.07	0.14 ± 0.08	2.56 ± 0.56	9.02 ± 0.61	-38 ± 13
158	WN+OB?	2	8.64	8.20	7.81	$0.84^{+0.16}_{-0.28}$	0.40 ± 0.03	6.46 ± 1.38	12.23 ± 1.40	31 ± 3

(1) Gamen et al. (2009), (2) van der Hucht (2001), (3) Gosset et al. (2001), (4) Gamen et al. (2014), (5) Davis, Moffat & Niemela (1981), (6) Fahed & Moffat (2012), (7) Lépine et al. (2001), (8) Williams et al. (1992): average of quiescent photometry in 1989, and (9) Varricatt & Ashok (2006).

to the near-IR. However, the paucity of published line strengths typically results in a flux ratio only being determinable in one near-IR band. When this is the case, we either adopt A_v from the literature (indicated in Tables 8 and 9) or exclude the star from our analysis.

To determine the nature of late-WC stars displaying diluted emission lines, we incorporate photometry from the *WISE* all-sky survey (Wright et al. 2010) allowing us to construct a simplistic 1-22 μm SED. We interpret a peak energy output at $\gtrsim 5$ μm as evidence for circumstellar dust emission, and stars displaying this are excluded from our analysis as we cannot determine their distances accurately. We identify only one line-diluted late WC, WR 42 (WC7+O7V), to be conclusively dust-free, and include this star in the binary field sample (Table 9) with J-band photometry corrected for the companion.

Our field WR star sample consists of 246 objects; 18 of these are corrected for a companion by the line-dilution technique, and 3 are corrected for a spectrally classified companion. We note that with the currently known population standing at ∼635, approximately 260 WR stars are unaccounted for in our calibration and field samples. Of these, the majority have uncertain spectral types, and lack spectra of sufficient quality (or spectral range) to obtain the required precision. Also excluded are stars with inconclusive evidence for a companion, and subtypes for which we cannot assign reliable near-IR absolute magnitudes (dusty WC stars, WN/C stars, WN10–11 stars).

A complete list of WR stars discovered between the Annex to the VIIth WR catalogue (van der Hucht 2001, 2006) and 2014 March is provided in Appendix A, which also highlights those for which distances have been obtained from the present study, together with an explanation of the revised nomenclature.

3.2 Spatial properties

The Galactic locations of 354 WN and non-dusty WC stars comprising our calibration and field samples are shown in Fig. 3. Uncertainties on distance moduli of field WR stars are displayed in Fig. 4, where it can be seen that $\Delta DM \sim 0.4$ mag typically applies, and minimum distance uncertainties are approximately ±14 per cent.

3.2.1 Radial distribution

Fig. 5 shows the radial distribution of 354 WR stars in the Milky Way. As expected, the majority of WR stars are located at Galactocentric distances of 3.5–10 kpc, with an additional peak at $R_G < 500$ pc owing to significant star formation within the central molecular zone (CMZ), reminiscent of OB star-forming regions (Bronfman et al. 2000).

Two conspicuous subpeaks, consisting mostly of WN stars, occur at $R_G \sim 4.5$ and ∼7.5 kpc. Both may be viewed as superpositions on the underlying WR population, the innermost and outermost are largely attributable to the WR content of Westerlund 1 (∼20 WR) and the nearby Cygnus star-forming region (∼15 WR, $l \sim 75^\circ$, $d = 1.3$–1.9 kpc), respectively.

3.2.2 z-distribution

Fig. 6 shows that, as expected, WR stars are largely confined to the thin disc. This strict confinement to $z = 0$ resembles a Cauchy distribution. Indeed, a non-linear least-squares fit of a Lorentzian function

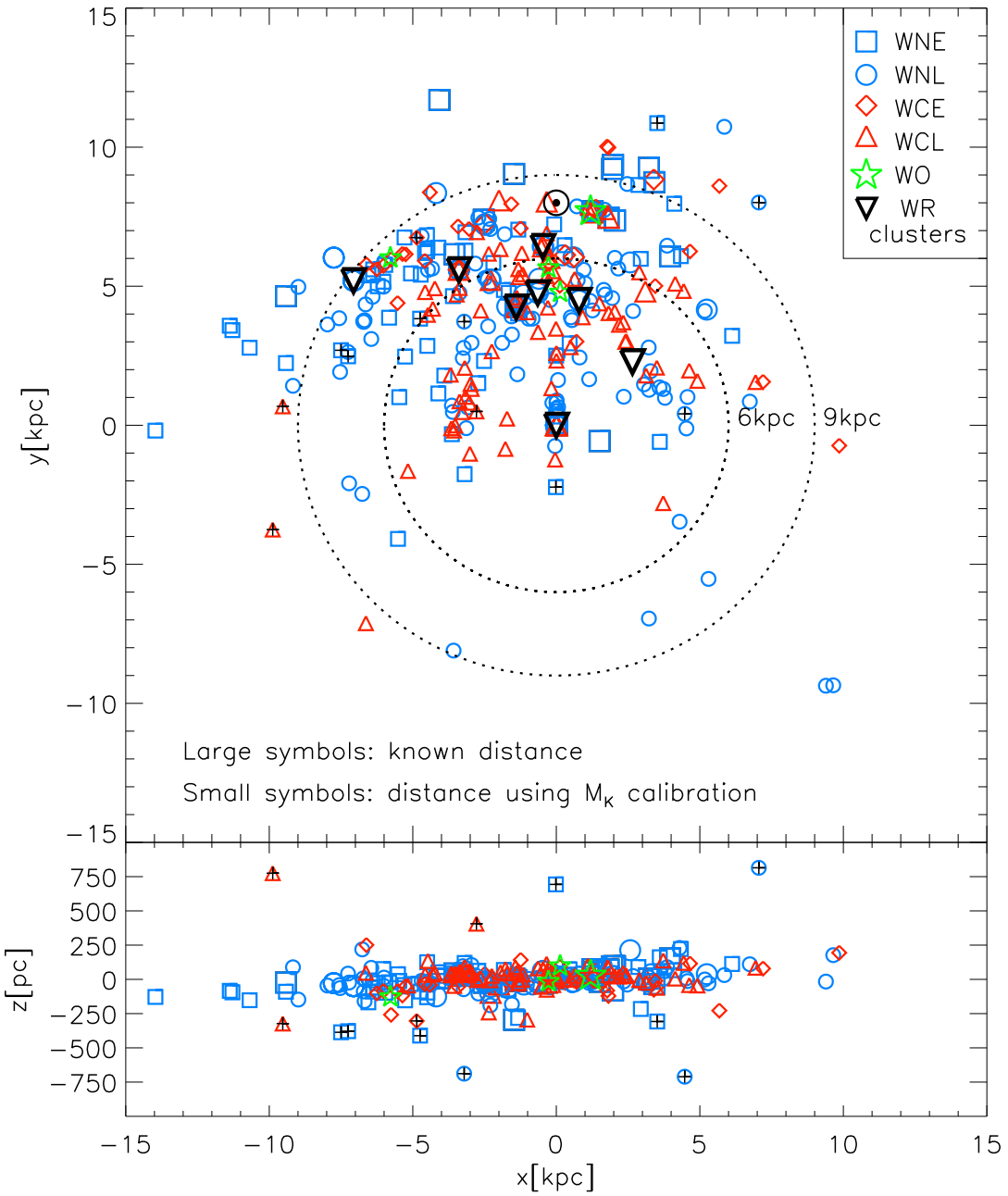

Figure 3. Positions of 354 WR stars projected on the Galactic plane (top) and viewed edge-on (bottom) in Cartesian coordinates, with the GC at (0, 0, 0). Galactic longitude increases anticlockwise about the Sun, which is represented by the standard symbol. Stars with known distances (calibration sample) are represented by larger symbols, whereas those with photometric distances (field sample) are represented by smaller symbols. Stars located at $|z| > 300$ kpc are marked with black crosses. The dotted lines at $R_G = 6$ and 9 kpc delineate the three chosen metallicity zones. From left to right, the displayed clusters from which > 1 WR stars are taken are: NGC 3603 [–7.07, 5.20], Danks 1 and 2 [–3.39, 5.59], Westerlund 1 [–1.40, 4.25], Halven–Moffat 1 and 2 [–0.65, 4.76], NGC 6231 [–0.47, 6.43], GC [0.0, 0.0], Arches and Quintuplet [0.02, 0.0], Cl 1813−178 [0.79, 4.49] and Quartet [2.65, 2.29].

(equation 8) matches well the distribution of vertical heights (z) of WR stars from the Galactic plane,

$$N(z) = A\left[\frac{\gamma^2}{(z - z_o)^2 + \gamma^2}\right], \quad (8)$$

where γ is the half-width at half-maximum (HWHM), z_o is the location of the peak and A is an intensity. Assuming the Sun lies 20 pc above the Galactic plane (Humphreys & Larsen 1995), our fit yields $\gamma = 39.2$ pc and $z_o = 1.9$ pc (Fig. 6).

Unlike other young stellar population tracers, we find no evidence for flaring of the WR star disc with increasing R_G, although this is likely due to the small number of WR stars identified beyond the solar circle. Paladini, Davies & De Zotti (2004) perform a Gaussian fit to the z-distribution of 456 Galactic H II regions interior to the solar circle, finding $\sigma \simeq 52$ pc (full width at half-maximum, FWHM $\sim$ 125 pc). Although not identical to the form of our fit, this distribution is broader than what we observe for WR stars. The thickness of the OB star-forming disc interior to the solar circle is measured by Bronfman et al. (2000), who find a FWHM of

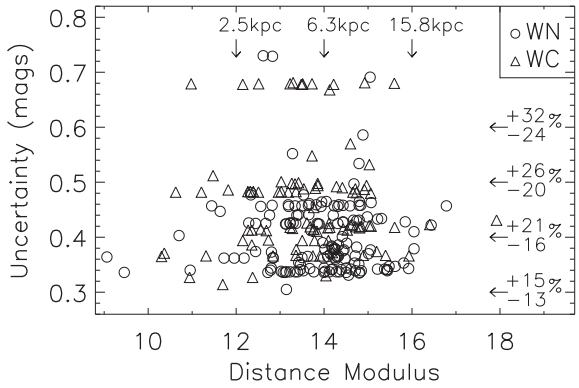

Figure 4. Distance modulus uncertainty for field WR stars, with equivalent distances indicated by vertical arrows and percentage errors by horizontal arrows.

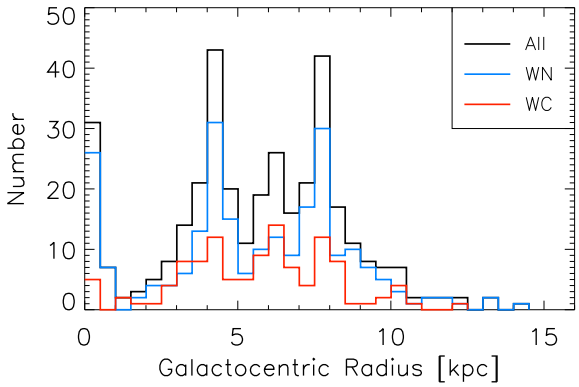

Figure 5. The distribution of Galactocentric radii for 354 WR stars, in 0.5 kpc bins.

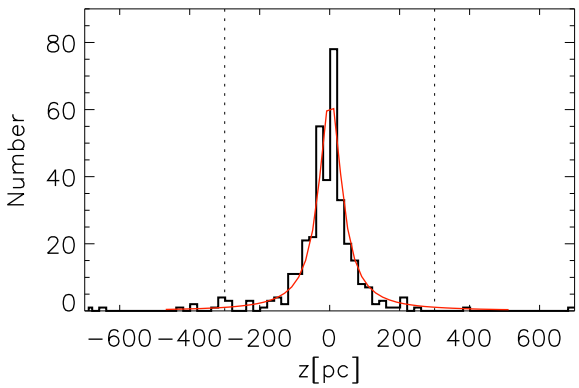

Figure 6. z-distribution of 354 Galactic WR stars shown in 20 pc bins (thick black line) with a fitted three-parameter Lorentzian function (thin red line, equation 8). Stars at $|z| > 300$pc (outside dotted lines) are listed in Table 10.

30–50 pc – slightly narrower than the WR star disc – flaring to > 200 pc beyond $R_G = 12$ kpc.

3.2.3 WR stars at large distances from the Galactic disc

A small fraction of WR stars are found at high vertical distances from the Galactic disc. Additional details of the 12 WR stars at $|z| > 300$ pc ($\gtrsim 7\gamma$) are shown in Table 10, all of which are presumably runaways from star formation sites in the thin disc. We include WR 124 in Table 10 since it has previously been identified as an extreme runaway by its high peculiar radial velocity (156 km s^{-1}; Moffat, Lamontagne & Seggewiss 1982). Here, we briefly discuss the possible events leading to their runaway status, and summarize the evidence for each.

First, we address the possibility that some of these objects are much fainter (thus less distant) WR-like central stars of planetary nebulae (CSPN). Both WC-like ([WC], e.g. Depew et al. 2011) and WN-like ([WN], e.g. Miszalski et al. 2012; Todt et al. 2013) CSPN have been observed in the field, although [WC]-type are far more common. These objects are almost identical in spectral appearance to their high-mass analogues (Crowther, Morris & Smith 2006b), yet are intrinsically fainter by several magnitudes.

We conduct a search for nebulosity around each $|z| > 300$ pc WR star by inspection of SuperCOSMOS Hα images (Parker et al. 2005) and any other published Hα imaging. Identification of a surrounding nebula cannot alone prove any of these objects to be CSPN, as some WR stars are seen to possess ejecta nebulae (Stock & Barlow 2010), yet it would provide a strong indication. Nebulosity is only observed around WR 71, which is known to be a genuinely massive, potential WR+compact object binary system (Isserstedt, Moffat & Niemela 1983). We therefore conclude that none of these 12 high-z WR stars are misclassified CSPN.

There are two leading mechanisms by which massive stars can be ejected from their birthplaces; the binary SN scenario where a massive binary system becomes unbound after an SN explosion (Blaauw 1961), and the dynamical ejection scenario where close encounters in a dense cluster can eject massive single or binary stars (Poveda, Ruiz & Allen 1967).

A WR star at $|z| = 700$ pc (similar to the highest observed), assuming $z = 0$ at birth and a time since ejection of 5 Myr (typical WR star age), would require an average velocity in the z-direction of 140 km s^{-1}. In the case of dynamical interaction between massive single and binary stars, a typical ejection velocity is given by $v_{ej}^2 = GM_b/a$ (M_b = total mass of binary with semimajor axis a) according to Fujii & Portegies Zwart (2011), and the ejected star usually has the lowest mass of 3. By this reasoning, assuming a $M \gtrsim 25\,M_\odot$ WR progenitor limit, a $M_b = 50\,M_\odot$ ($160\,M_\odot$) binary with a period up to 170 d (550 d) would be capable of ejecting a WR progenitor star with at least $v_{ej} = 140$ km s^{-1}. Ejection of the binary system is also possible in such an interaction, which one might expect thereafter to be associated with considerable hard X-ray flux from the collision of stellar winds. In Table 10, we include available X-ray observations for these 12 stars, showing that only WR 3 is conspicuous, lying on the L_X/L_{bol} relation for spectroscopic O-star binaries (Oskinova 2005). However, Marchenko et al. (2004) find no evidence for short period (<2 yr) radial velocity changes, concluding that WR 3 is likely a single star.

Alternatively, the locations of these stars may be explained by momentum gained from the SN explosion of a companion. Dray et al. (2005) estimate that 2/3 of massive runaways are produced this way. Isserstedt et al. (1983) show that kick velocities of ~ 150 km s^{-1} may be imparted on a surviving star, and that this star and the resulting SN remnant may remain bound if less than half the total system mass is lost during the SN. Therefore, one would expect a fraction of massive runaway stars to have compact companions. Indeed, WR 148 is an SB1 (Drissen et al. 1986) and the strongest Galactic candidate after Cyg-X3 for a WR+compact object binary. Low amplitude photometric and spectroscopic variations have been observed in WR 71 and WR 124 (Isserstedt et al. 1983; Moffat et al. 1982), suggesting they may also be SB1 systems with small mass functions. However, the absence of X-ray emission from accretion on to a compact object remains unexplained in all three cases. We

Table 10. Properties of 12 WR stars observed at $|z| > 300$ pc, plus WR 124 which is known to be an extreme runaway.

WR#	Spectral type	z (pc)	Binary status	L_X (ergs s^{-1})	Hα nebula?	Natal cluster
17	WC5	-303 ± 59	Single	Not detected[a]	–	–
3	WN3ha	-308 ± 83	Single	2.5×10^{32}[b]	–	–
56	WC7	-323 ± 58	Single	Not detected[a]	No	–
54	WN5	-378 ± 61	Single	Not detected[a]	No	–
49	WN5(h)	-386 ± 63	Single	Not detected[a]	No	–
75c	WC9	406 ± 78	Single	–	No	–
61	WN5	-411 ± 66	Single	$<5.0 \times 10^{30}$[b]	No	G305?
71	WN6	-689 ± 139	Binary? (SB1)[c]	Not detected[a]	Yes[d]	–
93a	WN3	694 ± 214	Single	–	No	GC?
123	WN8	-711 ± 120	Single	Not detected[a]	No	–
64	WC7	775 ± 127	Single	Not detected[a]	No	–
148	WN8h	814 ± 131	Binary (SB1)[e]	$<1.6 \times 10^{32}$[b]	–	–
124	WN8h	213 ± 39	Single	$<2.0 \times 10^{32}$[b]	Yes[d]	–

[a]*ROSAT* (Pollock, Haberl & Corcoran 1995), [b]Oskinova (2005), [c]Isserstedt et al. (1983), [d]Stock & Barlow (2010), and [e]Drissen et al. (1986).

note that the WR+OB binary fraction amongst this sample is very low, and quite possibly zero.

It has been suggested that WN8–9 subtypes are more frequently observed as WR runaways (Moffat 1989). If we consider only the most extreme examples, i.e. $|z| > 500$ pc plus WR 124, it can be seen from Table 10 that 3/6 are of the WN8 subtype. Although numbers are small, a preference seems to exist for WN8 runaways. Moffat (1989) argue that a WN8 spectral appearance may arise from mass accretion from a binary companion. Combined with the unusually low WR+OB binary fraction and the low-mass companion of WR 148, this evidence favours a binary SN origin for the extreme runaway WR population.

Two of the runaway stars listed in Table 10, WR 61 and WR 93a, are observed at similar Galactic longitudes to the G 305 complex and GC clusters, respectively. Considering our typical distance uncertainties (Fig. 4), ejection from these massive star-forming regions is a possible explanation for their large distance from the Galactic plane.

3.3 Subtype distributions across the Galactic metallicity gradient

Here, we assess how WR subtypes vary across the Milky Way disc and compare this to the predictions of metallicity (Z)-dependent evolutionary models. By including WR stars in the Large and Small Magellanic Clouds (LMC and SMC), we may probe massive star evolution over a metallicity range $Z = 0.002$–0.04. A constant SFR is implicitly assumed in all regions considered, allowing us to relate the relative numbers of WR subtypes observed with the relative duration of associated phases.

We proceed by dividing the Galaxy into three broad zones of supersolar ($R_G < 6$ kpc), solar ($6 < R_G < 9$ kpc), and subsolar ($R_G > 9$ kpc) metallicity. Based on the H II-region metallicity analysis of Balser et al. (2011), we assign approximate oxygen abundances ($\log[O/H] + 12$) of 8.85, 8.7 and 8.55 (± 0.1 dex) to each zone, respectively; each value is arrived at by inspection of their fig. 8 and a derived (azimuthally averaged) $\log[O/H]$ gradient of -0.05 ± 0.02 dex kpc^{-1}. According to our distribution analysis of 354 WR stars, we find 187, 132 and 35 to inhabit the supersolar, solar, and subsolar metallicity zones, respectively. Additionally, there are 148 known WR stars in the LMC (Breysacher, Azzopardi & Testor 1999; Neugent, Massey & Morell 2012, and references therein; Massey et al. 2014) for which the oxygen abundance is $(\log[O/H] + 12) = 8.38$ (Rolleston, Trundle & Dufton 2002), and 12 WR stars in the SMC (Massey & Duffy 2001; Massey, Olsen & Parker 2003) for which $(\log[O/H] + 12) = 8.13$ (Rolleston et al. 2003).

As recently highlighted by Groh et al. (2014), there is not a straightforward correspondence between spectroscopic and evolutionary phases in massive stars, particularly post-MS. Spectroscopically, any WN showing surface hydrogen (WN#h or (h)) or with ionization type ≥ 7 is identified as late-type (WNL), while H-free WN of ionization type ≤ 6 or those displaying broad emission lines (WN#b) are early type (WNE). We follow these definitions here, noting that the lack of near-IR hydrogen diagnostics is unlikely to significantly affect our measured N_{WNE}/N_{WNL}, as Galactic WN ≤ 7 stars are generally H-free (Hamann et al. 2006), so division by ionization type alone is sufficient. This assumption is less applicable in the lower metallicity regions of the outer Galaxy, however, low extinction in these directions means optical (hydrogen) diagnostics are commonly available. We include the WNha stars as WNL when evaluating subtype number ratios; their definition as such has minimal effect as only 18/235 WN considered belong to this class. The division in WC stars is more straightforward, with WC4–6 defined as early (WCE) and WC7–9 as late type (WCL). In Table 11, we show the subtype breakdown of WR stars observed in each Galactic metallicity region.

In stellar models, stars have historically been matched with the aforementioned spectroscopic WR types using basic surface abundance and effective temperature (T_{eff}) criteria. For example, Meynet & Maeder (2005) employ $T_{eff} > 10^4$ K and $X_H < 0.4$ as the definition of a WR star in their models, while Eldridge, Izzard & Tout (2008) add a further constraint of $\log(L/L_\odot) > 4.9$. This T_{eff} boundary is too low, since even the coolest WR stars (WN8–9) are found to have $\log(T_{eff}) \simeq 4.6$ (Hamann et al. 2006). A surface temperature of 10^4 K is more typical of late-B/early-A supergiants (Przybilla et al. 2006). Also, recent spectroscopic analysis of WC stars by Sander et al. (2012) indicate that some WC9 stars are very close to this lower luminosity limit. The transition between eWNE and eWNL phases (where 'e' denotes the definition in evolutionary models) is regarded to occur when $X_H < 10^{-5}$, and the eWC phase begins when carbon dominates nitrogen by mass (Meynet & Maeder 2005). By computing model spectra from evolutionary models, Groh et al. (2014) have shown that spectroscopic WNE and WNL lifetimes

Table 11. Observed WR number ratios in the Galaxy, LMC and SMC. Galactic WC stars counted here show no evidence of circumstellar dust, results incorporating an estimated 28 per cent of neglected (dusty) WC stars are parenthesized. The four WO stars are counted as WCE. An indication of uncertainty is given assuming $\sqrt{N}$ errors on each count.

Region (log [O/H] + 12)	N_{WR}	N_{WC} (N_{WCd})	N_{WN}	N_{WC}/N_{WN} ($N_{(WC+WCd)}/N_{WN}$)	N_{eWNE}/N_{eWNL}	$N_{(WCE+WO)}/N_{WCL}$
Inner Galaxy	187	63	124	0.51 ± 0.08	0.23 ± 0.05	0.05 ± 0.03
(8.85 ± 0.1)		(~ 22)		(0.69)		
Mid-Galaxy	132	46	86	0.53 ± 0.10	0.79 ± 0.17	1.0 ± 0.28
(8.7 ± 0.1)		(~ 16)		(0.73)		
Outer Galaxy	35	10	25	0.40 ± 0.16	1.27 ± 0.58	1.5 ± 0.97
(8.55 ± 0.1)		(~ 4)		(0.57)		
LMC	148	26	122	0.21 ± 0.05	1.93 ± 0.37	26/0
(8.38 ± 0.05)						
SMC (8.13 ± 0.05)	12	1	11	0.10 ± 0.09	11/0	1/0

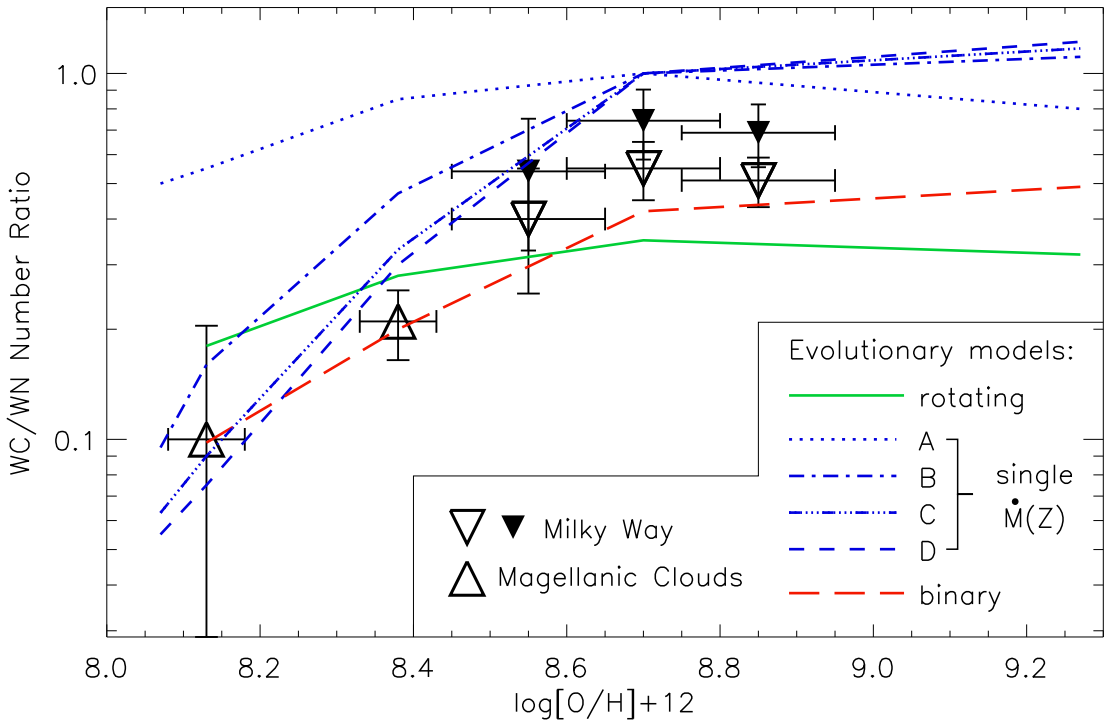

Figure 7. Number ratio of WC/WN stars in the LMC and SMC (triangles), and across three Milky Way regions (upsidedown triangles) where results omitting dusty WC stars (as in Table 11) are plotted as larger open symbols and smaller filled symbols represent the case where 28 per cent of all WC stars possess hot circumstellar dust (Section 4.3.2). The solid (green) line shows the predictions of Meynet & Maeder (2005) for rotating single stars. Long-dashed (red) line shows the predictions of Eldridge et al. (2008) for a population of massive binaries. All other lines (blue) represent non-rotating single-star evolutionary predictions of Eldridge & Vink (2006) for four different $\dot{M}-Z$ dependences. Errors on the number ratios shown are estimated assuming $\sqrt{N}$ counting errors in N_{WC} and N_{WN}. An uncertainty of 0.1 dex is assigned to each Galactic O/H value.

can differ radically from eWNE and eWNL lifetimes, as a star may have a WNE spectrum while retaining some surface hydrogen, hence this is a poor indicator. The problem is not so severe regarding the transition from WN to WC stars, as the change in surface carbon abundance is a rapid process, meaning the eWC phase corresponds well to the spectroscopic WC phase.

3.3.1 Incompleteness of the sample

Before comparing observed numbers with evolutionary model predictions, it is necessary to comment on two selection effects – one in our distribution analysis and one inherent to WR star surveys – that affect the star counts we present.

First, as we cannot assume reliable near-IR absolute magnitudes for dusty WC stars they have been excluded from our distribution analysis. Thus, in Table 11 we count only those WC stars showing no evidence for circumstellar dust. However, by inspection of a local volume-limited (<3 kpc) sample of WR stars (see Section 4.3.2 for full details), we estimate that 27($\pm$ 9) per cent of WC stars show evidence of circumstellar dust. To account for the effect of these neglected stars, we plot in Fig. 7 a set of enhanced WC/WN number ratios along with the values shown in Table 11. As this information is only available in the solar neighbourhood, we are forced to assume an unvarying fraction of dust-forming WC stars across the whole Galaxy. Late-type WC stars are known to dominate at higher metallicity, and it is predominantly these that are seen forming dust,

hence we expect this fraction in reality to be higher towards the GC. The slight downturn in $N_{\rm WC}/N_{\rm WN}$ at $R_{\rm G} < 6$ kpc could be due to a higher number of late-WC stars omitted from our analysis in this region.

Secondly, the two most widely employed WR star survey techniques are both least effective at identifying weak-lined WNE stars. Narrow-band IR imaging surveys are biased against WNEs due to low photometric excesses from their weak emission lines. The IR excess emission from free–free scattering – exploited by broad-band selection techniques – is also weaker in WNE stars as their wind densities are lower than other WR subtypes. For these reasons, and considering their modest IR luminosities, we expect WNE stars to be slightly underrepresented in our total sample, especially beyond the solar neighbourhood. Therefore, future observations will likely refine the numbers presented here by marginally decreasing $N_{\rm WC}/N_{\rm WN}$ and increasing $N_{\rm WNE}/N_{\rm WNL}$.

3.3.2 *Comparison to evolutionary predictions*

In Fig. 7, we plot observed $N_{\rm WC}/N_{\rm WN}$ in different regions of the Galaxy, and the Magellanic Clouds, alongside the predictions of various evolutionary models for massive stars. Rotating single-star models are taken from Meynet & Maeder (2005), non-rotating single-star models with various $\dot{M}(Z)$ dependences are taken from Eldridge & Vink (2006), and finally predictions for a population of non-rotating massive binaries exhibiting metallicity dependent mass-loss are taken from Eldridge et al. (2008) (BPASS).[2]

All models predict an increasing number of WC compared to WN stars with metallicity, due to increasingly rapid exposure of nuclear burning products caused by stronger stellar winds in more metal-rich environments. Our analysis shows only a modest variation of $N_{\rm WC}/N_{\rm WN}$ (0.4–0.55) across the Galactic disc, whereas the ratio drops considerably to 0.2–0.1 at LMC and SMC metallicities. At all metallicities the observed $N_{\rm WC}/N_{\rm WN}$ lies between the predictions from a population of binary stars (Eldridge et al. 2008) and single non-rotating stars. The addition of an estimated 28 per cent of neglected (dusty) WC stars at Galactic metallicities does not significantly alter this. However, the predictions of evolutionary models including rotation lie ubiquitously lower than our observations at Galactic metallicities. Fast rotation has the effect of lengthening WR lifetimes, manifest predominantly in the eWNL phase, thus reducing $N_{\rm WC}/N_{\rm WN}$ (Meynet & Maeder 2005). However, it is not expected that all massive stars are formed rotating as quickly ($v_i^{\rm rot} = 300$ km s^{-1}) as those generated in these models (Penny & Gies 2009).

Fig. 8 shows the number ratio of early- to late-WN stars in each Galactic metallicity zone, as well as in the LMC and SMC. An increase in the proportion of WNE can be seen with decreasing metallicity, and no WNL stars are known in the SMC. Contrary to this, the rotating models of Meynet & Maeder (2005) produce a *shorter* relative eWNE phase at lower metallicity, due to less efficient removal of the H-rich stellar envelope during prior evolutionary phases. Furthermore, rotationally induced mixing allows stars to become WR earlier in their evolution and experience an extended eWNL phase. The extreme sensitivity of the eWNE/eWNL transition to the chosen hydrogen surface abundance criterion clearly has a major influence on predictions (Groh et al. 2014). Therefore, we interpret the disparity shown in Fig. 8 largely as a symptom of these definitions rather than a serious conflict with evolutionary theory.

[2] http://www.bpass.org.uk/

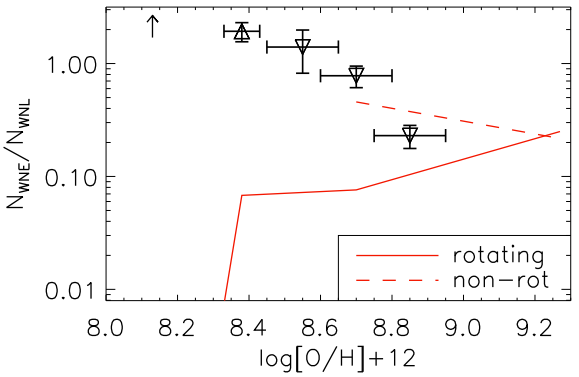

Figure 8. Number ratio of WNE/WNL stars across three metallicity zones in the Milky Way, LMC and SMC. The red lines show eWNE/eWNL predictions from rotating (solid) and non-rotating (dashed) evolutionary models (Meynet & Maeder 2005).

Our results show that the WN phase of WR stars at subsolar metallicities is almost entirely spent with a WNE spectral appearance, whereas the WNL spectral type endures longer on average at supersolar metallicities.

4 MODELLING THE TOTAL WR STAR POPULATION OF THE MILKY WAY

With knowledge of how WR subtypes vary with Galactocentric radius, and the intrinsic near-IR brightness of each subtype, we are in a position to model the observational properties of the whole Galactic WR population. To this end, we develop a 3D, azimuthally symmetric 'toy' model of the WR population – described in the following section – that is scalable to different total numbers of WR stars. For varying numbers of WR stars, we apply a simple Galactic dust distribution to redden the population, and derive magnitude distributions in various bands for comparison with the observed population, allowing us to estimate the total number of Galactic WR stars.

4.1 Populating the model

We do not attempt to incorporate complex structural features such as spiral arms or the Galactic bar into this model WR population, as our aim is to derive basic observational characteristics of the whole population, smoothing over any local enhancements. We therefore distribute model WR stars in an azimuthally symmetric disc, with the same thickness as the observed population. We generate the z-coordinate of each star so they are Cauchy distributed, by computing

$$z_i = \gamma \tan\left(\pi r_{01} - \frac{1}{2}\right), \qquad (9)$$

where r_{01} is a randomly generated number between 0 and 1 and γ is the observed HWHM (39.2 pc, Section 3.2.2). The z-distribution is truncated at $z = \pm 1$ kpc in accordance with the most extreme runaway stars observed.

We construct a model WR disc composed of 24 annuli of 0.5 kpc in width spanning radii $R_{\rm G} = 3$–15 kpc. Rather than using our observed radial distribution of WR stars to dictate the relative number in each annulus, we utilize a normalized version of the radial H II-region distribution presented by Paladini et al. (2004), since we consider H II regions to be a more complete tracer of hot young stars over a larger Galactic extent. Within each annulus, the model

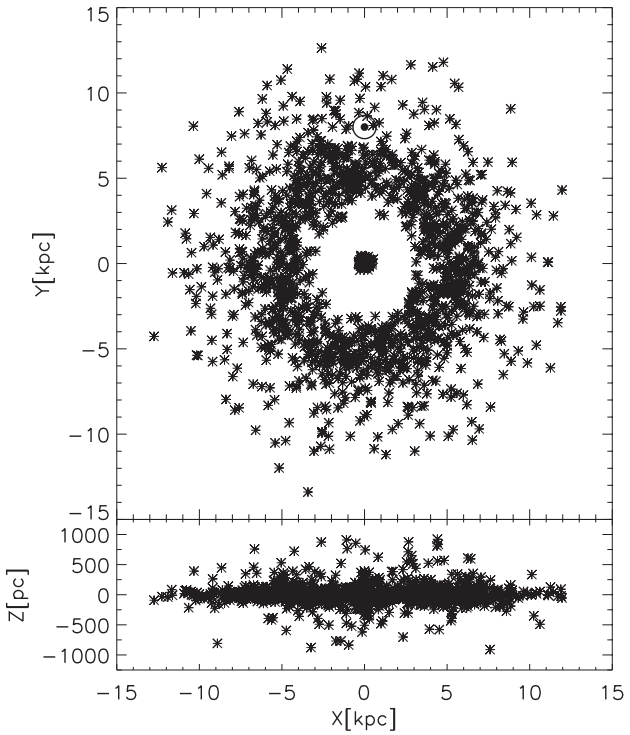

Figure 9. An example model WR population mimicking that of the Galaxy, containing 1050 stars at R_G = 3–15 kpc and 250 at R_G < 3 kpc, shown in Cartesian coordinates. The location of the Sun is indicated by the standard symbol at (0, 8 kpc) in the top panel.

stars are randomly placed between the lower and upper radii at a random angle (θ) between 0 and 2π around the model disc. In these coordinates, the Sun is located at $z = 20$ pc, $\theta = 0°$, and $R_G = 8000$ pc.

Interior to $R_G = 3$ kpc, where star formation is suppressed (aside from the CMZ) we include a fixed number of WR stars in every model. Dong et al. (2012) report on a Paα survey covering the central $\sim 0.^{\circ}6$ (~ 80 pc) of the Galaxy, including the three massive clusters (Arches, Quintuplet and GC). Within this region they identify as many emission line sources (evolved massive star candidates) outside of these clusters as within them; given that ~ 80 WR stars are known to reside in these clusters, we estimate 160 WR stars present in the Dong et al. survey area. The CMZ is approximately 3° (400 pc) across, and the density of gas in this extreme environment is strongly centrally peaked, so that approximately 40 per cent of the CMZ gas lies within the Dong et al. survey area (Ferrière 2008). Assuming the non-cluster population of WR stars roughly follows the amount of molecular gas, this would imply a further ~ 100 WR stars in the CMZ. The inner Galaxy ($R_G < 3$ kpc) contains little star formation outside the CMZ, we therefore populate this area in our models with 250 WR stars, following a Gaussian distribution centred on $R_G = 0$ with $\sigma = 200$ pc. An example model is displayed in Fig. 9.

The number of WR stars in each radial bin of our model population is divided into four components representing WNE, WNL, WCE and WCL. The relative numbers of each WR type match those observed (Table 11), varying from the model GC where late types dominate to $R_G = 15$ kpc where early types are in the majority. We assign absolute magnitudes of $M_{K_S} = -4.31, -6.01, -4.45$ and -4.89 to WNE, WNL, WCE, and WCL types, respectively, based on averaging our calibration results (Section 2.5). We do not include WO or WN/C stars as they constitute a negligible fraction of the population.

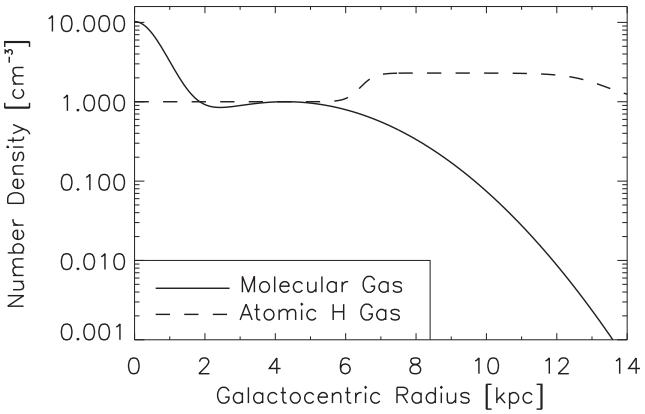

Figure 10. Mid-plane number density of molecular H_2 (solid) and atomic H (dashed) gas, used to govern our model dust distribution, as a function of Galactocentric radius (equations 11 and 12, respectively).

4.2 A dust model for the Milky Way

We include two dust components in our model WR star disc; one associated with molecular (H_2) gas, the other with atomic H gas. We apply the same dust-to-gas mass ratio for each component. This assumption follows Bohlin, Savage & Drake (1978) who derive a *total* neutral hydrogen to colour excess ratio, implying the each atom of H is responsible for a set amount of extinction, whether in molecular or atomic form. Both dust components are included as 2D functions in R_G and z, motivated by the spatial distribution measured for their respective gas species. These gas measurements are taken from Nakanishi & Sofue (2006) and Nakanishi & Sofue (2003) for molecular (traced using CO) and atomic gas, respectively.

Functions describing each dust component have the form $D_m(R_G) \times D_h(R_G, z)$, where $D_m(R_G)$ describes the dependence of mid-plane density on Galactocentric radius and $D_h(R_G, z)$ describes how the density drops with vertical distance from the mid-plane.

Both dust components are included with a vertical dependence of the form $D_h(R_G, z) = \mathrm{sech}^2(\zeta)$, where

$$\zeta(R_G, z) = \log(1+\sqrt{2})\frac{z}{z_{1/2}(R_G)} \tag{10}$$

and $z_{1/2}(R_G)$ is the height at which the density falls to half of the mid-plane value, which increases linearly with Galactocentric radius for both gas species. For molecular gas, $z_{1/2}(0) = 25$ pc increasing to 90 pc at $R_G = 10$ kpc (Nakanishi & Sofue 2006). For atomic gas, $z_{1/2}(0) = 100$ pc increasing to 500 pc at $R_G = 15$ kpc (Nakanishi & Sofue 2003).

To represent the mid-plane density of molecular gas, we construct the following function:

$$D_m^{\mathrm{mol}}(R_G) = N_0^{\mathrm{mol}}\mathrm{sech}^2\left(\frac{R_G}{800\,\mathrm{pc}}\right)\ldots + \exp\left[\frac{-(R_G - 4300\,\mathrm{pc})^2}{2(2500\,\mathrm{pc})^2}\right][\mathrm{cm}^{-3}], \tag{11}$$

which is shown in Fig. 10. The scaling values in equation (11) and $N_0^{mol} = 10\,\mathrm{cm}^{-3}$ are chosen to reproduce the maps of Nakanishi & Sofue (2006).

To represent the mid-plane density of atomic gas, we employ a summation of two step functions:

$$D_m^{\rm atom}(R_{\rm G}) = N_0^{\rm atom}\left[1 + \frac{1.3}{1+\exp(\frac{-(R_{\rm G}-6500\,{\rm pc})}{200\,{\rm pc}})}\cdots - \frac{1.3}{1+\exp(\frac{-(R_{\rm G}-13\,200\,{\rm pc})}{550\,{\rm pc}})}\right][{\rm cm}^{-3}] \quad (12)$$

as shown in Fig. 10. Once again, we choose the scaling values and $N_0^{\rm atom} = 0.08\,{\rm cm}^{-3}$ to reproduce the maps of Nakanishi & Sofue (2003).

Finally, we integrate the total dust function

$$D(R_{\rm G}, z) = (D_m^{\rm mol} \times D_h^{\rm mol}) + (D_m^{\rm atom} \times D_h^{\rm atom}), \quad (13)$$

along the line of sight from the Sun to each model WR star to provide a total amount of obscuring dust. Hence, we obtain an extinction to each model star, assuming A_{K_S} is proportional to the amount of dust along the line of sight, normalized to give $A_{K_S} = 2.42$ mag towards the GC ($R_{\rm G} = 0$, $z = 0$; Fritz et al. 2011).

4.3 Quantifying the total population

By combining our model WR star population (Section 4.1) with the dust function described in the previous section, we are able to generate a global magnitude distribution for a WR population containing any number of stars. The total WR star population follows an assessment of which predicted magnitude distribution most closely reproduces that observed.

Before deducing this number, it is worth reconsidering what the WR stars in our model represent. As their absolute magnitudes are based on our calibrated values for WR stars (Section 2), they represent what we will refer to as 'WR-dominated' systems, i.e. where any companion star(s) do not affect the systemic magnitude by more than 0.4 mag (typical error on our absolute magnitude calibrations), i.e. $(m_K^{\rm WR} - m_K^{\rm sys}) > 0.4$, corresponding to a WR/system flux ratio of $F_K^{\rm WR}/F_K^{\rm sys} > 0.7$. Also, these model stars do not represent WO, WN/C or dust-producing WC stars. Therefore, to achieve a like-for-like comparison to observations, we initially only consider observed 'WR-dominated' systems, and in Section 4.3.2 estimate the contribution of neglected WR types.

4.3.1 Comparison to a magnitude-limited sample

For comparison to our model K_S-band magnitude distributions, we assemble a magnitude-limited sample of real WR-dominated systems. We note that < 5 per cent of WR stars discovered since the year 2011 are brighter than $K_S = 8$ mag (Mauerhan et al. 2011; Shara et al. 2012; Smith et al. 2012; Chené et al. 2013). Therefore, we adopt this as the current completeness limit.

Fig. 11 presents predicted magnitude distributions for WR populations containing 850, 1050 and 1250 stars between $R_{\rm G} = 3$–15 kpc plus 250 central stars ($R_{\rm G} < 3$ kpc). Also shown is the number of observed WR-dominated systems with systemic $K_S < 8$ mag. In spite of providing too few systems with $7.5 < K_S < 8.0$, the best agreement is found with the 1050 + 250 WR star model. We take forward 1300 ± 200 as the number of Galactic WR-dominated systems, where the uncertainty is based on the comparison shown in Fig. 11.

As commented on previously (Section 2.5.1), assuming a shallower extinction law along lines of sight towards the GC has the effect of brightening our calibrated M_{JHK_S} values for late-type WN and WC stars by up to 0.3 mag. Upon altering the magnitudes of the late-type WR stars in our model population by this amount, we find more consistency with magnitude distributions drawn from models containing ∼150 fewer WR stars. Hence, the effect of a shallower GC extinction law is within the uncertainties.

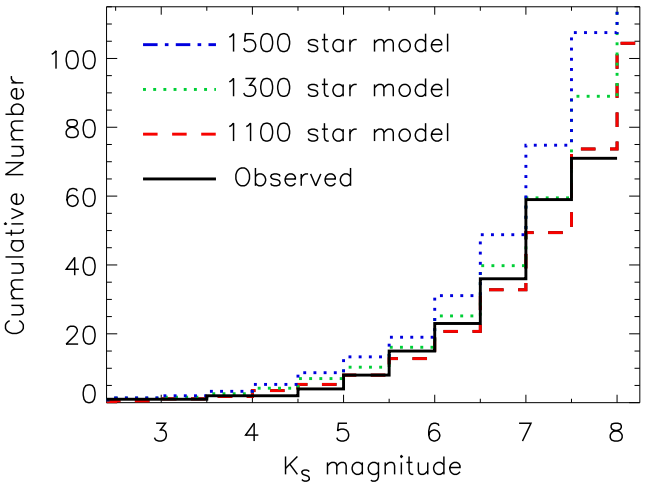

Figure 11. The cumulative number of observed WR-dominated systems (black solid line) in bins of 0.5 K_S mag, compared with that of three different model WR populations.

4.3.2 Fractions of dusty and companion-dominated WR systems in a volume-limited sample

Each point in our model WR star population represents a stellar system where a WR star is the dominant or sole near-IR source. To gain an insight into how many dusty and companion-dominated WR systems are overlooked by these models – and hence our initially deduced population of 1300 – we construct a volume limited sample of nearby WR systems. In Appendix D, we list all known WR stars within 3kpc of the Sun, where distances are taken from this work where possible (non-dusty WR stars), or by implementing $\bar{M}_v$-subtype calibrations of van der Hucht (2001). A v-band approach can be used to determine distances to dusty WC stars as hot dust emission does not contribute to the continuum flux at these wavelengths. We inspect the near-IR properties of these nearby WR stars, categorizing each as either WR-dominated ($F_K^{\rm WR}/F_K^{\rm sys} > 0.7$), having a significant companion ($F_K^{\rm WR}/F_K^{\rm sys} < 0.7$), or dusty WC.

Of the 72 WR stars in this volume-limited sample, 41 are WC type of which 11 show evidence of circumstellar dust, indicating that 15 ± 5 per cent of WR stars and 27 ± 9 per cent of WC stars display circumstellar dust. A companion star dominates the near-IR continuum in 11 of the remaining 61 non-dusty WR systems (18 ± 6 per cent). Uncertainties on these fractions are calculated assuming a $\sqrt{N}$ uncertainty on each number count.

Therefore, we may assume our previously derived population of 1300 represents only 82 per cent of the non-dusty population, as ∼18 per cent (300) will have an IR bright companion. Furthermore, this non-dusty population of 1600 (= 1300 + 300) represents only 85 per cent of the total population, as a further ∼15 per cent (300) will be dusty WC stars.[3] Hence we estimate the total number of Galactic WR stars at 1900 ± 250.

[3] On the basis of no Galactocentric radial dependence on the fraction of dust-producing WC stars.

4.4 Expectations from star formation arguments

By combining the measured Milky Way SFR with an initial mass function (IMF), it is possible to derive the average lifetime of the WR phase ($\tau_{\rm WR}$) necessary to sustain a population of ∼1900 WR stars. Taking the Milky Way SFR to be 1.9 $M_\odot$ yr^{-1} (Chomiuk & Povich 2011), adopting a three-part Kroupa IMF (Kroupa & Weidner 2003), and assuming only stars with an initial mass > 25 $M_\odot$ experience a WR phase, our derived population can be reproduced with $\tau_{\rm WR} \simeq$ 0.4 Myr.

This result is broadly consistent with rotating (non-rotating) Geneva models at solar metallicity (Georgy et al. 2012), which display $\tau_{\rm WR} = 0.45$ Myr (0.006 Myr) at $M_i = 32\,M_\odot$ increasing with mass to 0.9 Myr (0.4 Myr) at $M_i = 120\,M_\odot$. WR lifetimes as a result of binary evolution at solar metallicity (Eldridge et al. 2008) are predicted to span $\tau_{\rm WR} = 0.5$ Myr at $M_i = 30\,M_\odot$ to 1.0 Myr at 120 $M_\odot$, slightly above that implied by our estimated population, although binary evolution favours lower WR progenitor masses so that our model population may not correspond to all WR stars formed via this channel. Previously claimed population sizes of > 6000 (van der Hucht 2001; Shara et al. 2009) are difficult to reconcile with the measured Galactic SFR and a progenitor mass limit $M > 25\,M_\odot$, as WR lifetimes in excess of 1 Myr would be required.

The CMZ accounts for an estimated ∼4–5 per cent of Galactic star formation (Longmore et al. 2013), yet we estimate that it contains ∼250 (13 per cent) of the Galactic WR star population. The discrepancy between these fractions would suggest either we have underestimated WR numbers in the Galactic disc, or this CMZ SFR is insensitive to the most recent episodes of massive star formation.

4.5 Implications for future spectroscopic surveys

Near-IR surveys, both broad and narrow band, continue to add to our knowledge of the obscured Galactic WR population. A question of fundamental importance to spectroscopic follow-up campaigns, is how deep do spectroscopic surveys need to go? Fig. 12 shows multiband magnitude distributions derived from our favoured model WR star population. We estimate that to achieve 95 per cent completeness, spectra of candidate WR stars need to be taken to a depth of $K_S \simeq 17.5$ mag (17.4 [17.6] in models [not] including dusty WC stars), $H \simeq 23.3$ or $J \simeq 34.3$ – deeper by ∼2 mag in K than the 95 per cent limit estimated by Shara et al. (2009).

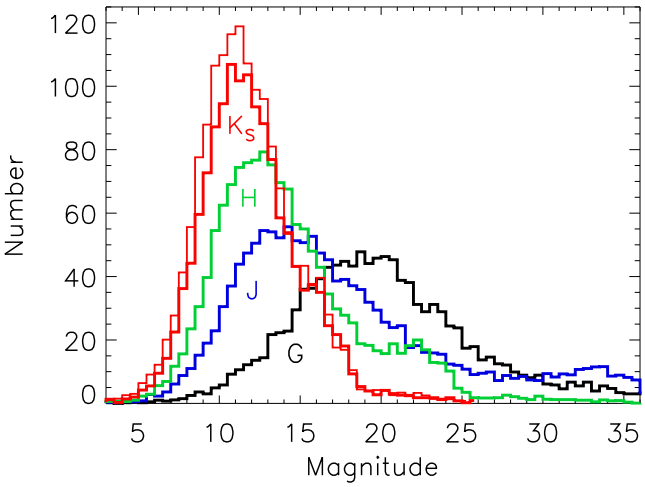

Figure 12. Histogram of multiband observables derived from our favoured model Galactic WR star population, averaged over 10 model repetitions, including 2MASS JHK_S and the G band of *Gaia*. Two K_S-band distributions are plotted, the thin (red) line represents a model population where 28 per cent of WC stars are dust forming (WC8d/9d, $M_{K_S} = -6.95$, Table 5). The thick (red, green, blue and black) lines all represent populations consisting of WN and non-dusty WC stars.

The ESA *Gaia* mission will perform precision astrometry for a billion stars down to visual magnitudes of 20, and acquire low-resolution spectra of objects brighter that magnitude 16. To investigate the potential of *Gaia* in the search for and characterization of WR stars, we derive the observed G-band distribution of our favoured model population (Fig. 12). To do this, we implement magnitude transformations provided by Jordi et al. (2010), M_v for WR stars from van der Hucht (2001), and $(b-v)_o$ colours from Morris et al. (1993). We predict that approximately 600 (∼ 1/3 of total) WR stars will appear within *Gaia*'s $6 < G < 20$ observing range, with ∼ 250 brighter than the magnitude limit for spectroscopy. With the known population currently totalling ∼ 635, *Gaia* is unlikely to discover significant WR populations via spectroscopy, but the majority of those known will have distances measured to a significantly higher level of accuracy than is currently possible.

5 CONCLUSIONS

We have presented near-IR absolute magnitude–spectral type calibrations for WN, WC and WO type WR stars, based on 126 examples with known distances (mostly by cluster or OB association membership). Applying these calibrations to the rapidly growing known Galactic population, we derive distances to a further 246 WR stars and present a 3D map of their locations. We note that approximately half as many WC stars are available for calibration as cluster/association members than WN, consistent with the findings of Smith & Tombleson (2015) than WC stars are generally more isolated. This challenges the idea that WC stars descend directly from WN, which in turn descend from the most massive O stars. We have shown the heights of WR stars from the Galactic mid-plane to be Cauchy distributed with HWHM = 39.2 pc, where 12 stars reside at $|z| > 300$ pc. The low binary fraction and a preference for WN8 subtypes in this small sample of runaway stars indicates a binary SN origin for the most extreme examples.

Exploiting the variation of metallicity across the Galactic disc, we have compared subtype number ratios measured in the inner Galaxy, solar neighbourhood, and outer Galaxy to the predictions of various metallicity-dependent evolutionary models. We measure $N_{\rm WC}/N_{\rm WN}$ to be significantly higher than predicted by evolutionary models including fast rotation (Meynet & Maeder 2005), suggesting that lengthened WNL and shortened WC phases resulting from stellar rotation are not widely observed at ($Z \gtrsim Z_\odot$). Similarly, a shortened eWNE phase in such models – particularly at lower metallicity – is not manifest in our observations, as we observe approximately equal numbers of WNE and WNL stars in regions of $Z \lesssim Z_\odot$. Single-star models without rotation (Eldridge & Vink 2006) and models that account for the various effects of binary interaction (Eldridge et al. 2008) reproduce our measurements of $N_{\rm WC}/N_{\rm WN}$ more appropriately. Hence, to a first approximation a population consisting of non-rotating single stars and interacting binaries would be consistent with the $N_{\rm WC}/N_{\rm WN}$ we observe. However, we caution that all comparisons of this nature are subject to how the physics contained in stellar models is expected to translate into observable properties, which currently rests on estimations of surface abundances and temperatures that may not be appropriate (Groh et al. 2014), particularly for the transition between eWNE and eWNL subtypes.

Consolidating information gained about the spatial distribution, subtype variation, and intrinsic IR brightness of WR stars, we have created a scalable toy model of the Galactic WR population. By applying a 3D dust distribution to this model – spatially congruous with the gas content of the Galaxy – we derive observable properties for populations of various sizes at multiple wavelengths. Comparison of these model-derived observables to the observed population of non-dusty, WR-dominated ($m_K^{\rm WR} - m_K^{\rm sys} > 0.4$) systems to a completeness limit of $m_K^{\rm sys} < 8$ indicates a total of $\simeq 1300$ in the Galaxy. Using a volume-limited sample ($d < 3$ kpc), we estimate that such systems represent ~ 69 per cent of the whole WR population, hence we claim a Galactic WR population totalling 1900 ± 250.

We deduce that an average WR phase duration of 0.4 Myr is necessary to sustain our estimated population, assuming a Kroupa IMF and a constant Milky Way SFR of 1.9 $M_\odot$ yr^{-1}. This is compatible with WR phase durations in rotating evolutionary models at solar metallicity (Georgy et al. 2012).

Looking to the future, we have used our favoured model WR population to estimate a required depth of $K_S < 17.5$ for spectroscopic surveys to achieve 95 per cent completeness in Galactic WR stars. We have also predicted that the ESA *Gaia* mission will not deliver a significant number of WR star discoveries via low-resolution spectroscopy, but should provide improved distance measurements for the majority of the currently recognized population.

ACKNOWLEDGEMENTS

The authors would like to thank the referee (A. F. J. Moffat) for a careful reading and useful comments that improved the paper. We also thank William. D. Vacca for making available high-quality spectra of selected WR stars, useful for refining near-IR classification diagnostics. We are also grateful to MPhys students Adrian Kus and Katie Baker for constructing and originally populating the Wolf–Rayet catalogue data base. This work was supported in part by a UK Science and Technology Facilities Council studentship (CKR).

REFERENCES

Anderson G. E. et al., 2011, ApJ, 727, 105
Arnal E. M., Cappa C. E., Rizzo J. R., Cichowolski S., 1999, AJ, 118, 1798
Balser D. S., Rood R. T., Bania T. M., Anderson L. D., 2011, ApJ, 738, 27
Baume G., Vázquez R. A., Carraro G., 2004, MNRAS, 355, 475
Benjamin R. A. et al., 2003, PASP, 115, 953
Bibby J. L., Crowther P. A., Furness J. P., Clark J. S., 2008, MNRAS, 386, L23
Blaauw A., 1961, Bull. Astron. Inst. Neth., 15, 265
Bohannan B., Crowther P. A., 1999, ApJ, 511, 374
Bohlin R. C., Savage B. D., Drake J. F., 1978, ApJ, 224, 132
Borissova J. et al., 2012, A&A, 546, A110
Bressert E. et al., 2010, MNRAS, 409, L54
Breysacher J., Azzopardi M., Testor G., 1999, A&AS, 137, 117
Bronfman L., Casassus S., May J., Nyman L.-Å., 2000, A&A, 358, 521
Burgemeister S. Gvaramadze V. V., Stringfellow G. S., Kniazev A. Y. Todt H., Hamann W.-R., 2013, MNRAS, 429, 3305
Cappa C. E., Goss W. M., Niemela V. S., Ostrov P. G., 1999, AJ, 118, 948
Cappa C. E., Vasquez J., Pineault S., Cichowolski S., 2010, MNRAS, 403, 387
Carraro G., Turner D., Majaess D., Baume G., 2012, in Proc. IAU Symp. 289, Beijing, preprint (arXiv:1209.2080)
Chené A.-N., Borissova J., Bonatto C., Majaess D. J., Baume G., Clarke J. R. A., Kurtev R., Schnurr O., 2013, A&A, 549, A98
Chené A.-N., Moffat A. F. J., St-Louis N., Schnurr O., Crowther P. A., Artiguau E., Alecian E., Wade G. A., 2014, MNRAS, submitted
Chomiuk L., Povich M. S., 2011, AJ, 142, 197
Clark J. S., Negueruela I., Crowther P. A., Goodwin S. P., 2005, A&A, 434, 949
Cohen M., Parker Q. A., Green A. J., 2005, MNRAS, 360, 1439
Conti P. S., Massey P., Vreux J.-M., 1990, ApJ, 354, 359
Corradi R. L. M. et al., 2010, A&A, 509, A41
Corti M., Bosch G., Niemela V., 2007, A&A, 467, 137
Cotera A. S., Simpson J. P., Erickson E. F., Colgan S. W. J., Burton M. G., Allen D. A., 1999, ApJ, 510, 747
Crowther P. A., 2003, Ap&SS, 285, 677
Crowther P. A., 2007, ARA&A, 45, 177
Crowther P. A., Smith L. J., 1996, A&A, 305, 541
Crowther P. A., Walborn N. R., 2011, MNRAS, 416, 1311
Crowther P. A., Smith L. J., Hillier D. J., Schmutz W., 1995a, A&A, 293, 427
Crowther P. A., Smith L. J., Hillier D. J., 1995b, A&A, 302, 457
Crowther P. A., De Marco O., Barlow M. J., 1998, MNRAS, 296, 367
Crowther P. A., Dessart L., Hillier D. J., Abbott J. B., Fullerton A. W., 2002, A&A, 392, 653
Crowther P. A., Hadfield L. J., Clark J. S., Negueruela I., Vacca W. D., 2006a, MNRAS, 372, 1407
Crowther P. A., Morris P. W., Smith J. D., 2006b, ApJ, 636, 1033
Davies B., de La Fuente D., Najarro F., Hinton J. A., Trombley C., Figer D. F., Puga E., 2012a, MNRAS, 419, 1860
Davies B. et al., 2012b, MNRAS, 419, 1871
Davis A. B., Moffat A. F. J., Niemela V. S., 1981, ApJ, 244, 528
de La Chevrotière A., Moffat A. F. J., Chené A.-N., 2011, MNRAS, 411, 635
de la Fuente D., Najarro F., Davies B., Figer D. F., 2013, in Guirado J. C., Lara L. M., Quilis V., Gorgas J., eds, Highlights of Spanish Astrophysics VII. Proceedings of the X Scientific Meeting of the Spanish Astronomical Society (SEA), p. 534, preprint (arXiv:1210.1781)
De Marco O., Schmutz W., 1999, A&A, 345, 163
Depew K., Parker Q. A., Miszalski B., De Marco O., Frew D. J., Acker A., Kovacevic A. V., Sharp R. G., 2011, MNRAS, 414, 2812
Djurašević G., Zakirov M., Eshankulova M., Erkapić S., 2001, A&A, 374, 638
Dong H., Wang Q. D., Morris M. R., 2012, MNRAS, 425, 884
Dray L. M., Tout C. A., Karakas A. I., Lattanzio J. C., 2003, MNRAS, 338, 973
Dray L. M., Dale J. E., Beer M. E., Napiwotzki R., King A. R., 2005, MNRAS, 364, 59
Drissen L., Lamontagne R., Moffat A. F. J., Bastien P., Seguin M., 1986, ApJ, 304, 188
Eikenberry S. S. et al., 2004, ApJ, 616, 506
Eldridge J. J., Vink J. S., 2006, A&A, 452, 295
Eldridge J. J., Izzard R. G., Tout C. A., 2008, MNRAS, 384, 1109
Eldridge J. J., Fraser M., Smartt S. J., Maund J. R., Crockett R. M., 2013, MNRAS, 436, 774
Espinoza P., Selman F. J., Melnick J., 2009, A&A, 501, 563
Esteban C., Peimbert M., 1995, A&A, 300, 78
Esteban C., Rosado M., 1995, A&A, 304, 491
Fahed R., Moffat A. F. J., 2012, MNRAS, 424, 1601
Fahed R. et al., 2011, MNRAS, 418, 2
Faherty J. K., Shara M. M., Zurek D., Kanarek G., Moffat A. F. J., 2014, AJ, 147, 115
Fang M. et al., 2012, A&A, 539, A119
Ferrière K., 2008, Astron. Nachr., 329, 992
Figer D. F., McLean I. S., Najarro F., 1997, ApJ, 486, 420
Figer D. F., McLean I. S., Morris M., 1999, ApJ, 514, 202
Fritz T. K. et al., 2011, ApJ, 737, 73
Fujii M. S., Portegies Zwart S., 2011, Science, 334, 1380
Gamen R. et al., 2006, A&A, 460, 777
Gamen R. C., Fernández-Lajús E., Niemela V. S., Barbá R. H., 2009, A&A, 506, 1269
Gamen R. C., Collado A., Barbá R., Chené A.-N., St-Louis N., 2014, A&A, 562, A13
Garmany C. D., Stencel R. E., 1992, A&AS, 94, 211

Georgy C., Ekström S., Meynet G., Massey P., Levesque E. M., Hirschi R., Eggenberger P., Maeder A., 2012, A&A, 542, A29
Gillessen S., Eisenhauer F., Fritz T. K., Pfuhl O., Ott T., Genzel R., 2013, in de Grijs R., ed., Proc. IAU Symp. 289, Advancing the Physics of Cosmic Distances. Cambridge Univ. Press, Cambridge, p. 29
Gosset E., Royer P., Rauw G., Manfroid J., Vreux J.-M., 2001, MNRAS, 327, 435
Groh J. H., Meynet G., Ekström S., Georgy C., 2014, A&A, 564, A30
Gvaramadze V. V. et al., 2009, MNRAS, 400, 524
Gvaramadze V. V., Kniazev A. Y., Hamann W.-R., Berdnikov L. N., Fabrika S., Valeev A. F., 2010, MNRAS, 403, 760
Hadfield L. J., van Dyk S. D., Morris P. W., Smith J. D., Marston A. P., Peterson D. E., 2007, MNRAS, 376, 248
Hamann W.-R., Gräfener G., Liermann A., 2006, A&A, 457, 1015
Hanson M. M., Kurtev R., Borissova J., Georgiev L., Ivanov V. D., Hillier D. J., Minniti D., 2010, A&A, 516, A35
Harayama Y., Eisenhauer F., Martins F., 2008, ApJ, 675, 1319
Hill G. M., Moffat A. F. J., St-Louis N., 2002, MNRAS, 335, 1069
Hillenbrand L. A., Massey P., Strom S. E., Merrill K. M., 1993, AJ, 106, 1906
Homeier N. L., Blum R. D., Pasquali A., Conti P. S., Damineli A., 2003, A&A, 408, 153
Hopkins P. F., Quataert E., Murray N., 2011, MNRAS, 417, 950
Howarth I. D., Schmutz W., 1992, A&A, 261, 503
Howarth I. D., Schmutz W., 1995, A&A, 294, 529
Humphreys R. M., Larsen J. A., 1995, AJ, 110, 2183
Hur H., Sung H., Bessell M. S., 2012, AJ, 143, 41
Hyodo Y., Tsujimoto M., Koyama K., Nishiyama S., Nagata T., Sakon I., Murakami H., Matsumoto H., 2008, PASJ, 60, 173
Indebetouw R. et al., 2005, ApJ, 619, 931
Isserstedt J., Moffat A. F. J., Niemela V. S., 1983, A&A, 126, 183
Jordi C. et al., 2010, A&A, 523, A48
Kanarek G. C., Shara M. M., Faherty J. K., Zurek D., Moffat A. F. J., 2014, AJ, preprint (arXiv:1403.0975)
Kendrew S. et al., 2012, ApJ, 755, 71
Kothes R., Dougherty S. M., 2007, A&A, 468, 993
Koumpia E., Bonanos A. Z., 2012, A&A, 547, A30
Kroupa P., Weidner C., 2003, ApJ, 598, 1076
Kurtev R., Borissova J., Georgiev L., Ortolani S., Ivanov V. D., 2007, A&A, 475, 209
Lada C. J., Lada E. A., 2003, ARA&A, 41, 57
Lejeune T., Schaerer D., 2001, A&A, 366, 538
Lépine S., Wallace D., Shara M. M., Moffat A. F. J., Niemela V. S., 2001, AJ, 122, 3407
Liermann A., Hamann W.-R., Oskinova L. M., 2009, A&A, 494, 1137
Littlefield C., Garnavich P., "Howie" Marion G. H., Vinkó J., McClelland C., Rettig T., Wheeler J. C., 2012, AJ, 143, 136
Longmore S. N. et al., 2013, MNRAS, 429, 987
Lortet M. C., Testor G., Niemela V., 1984, A&A, 140, 24
Lundström I., Stenholm B., 1984, A&AS, 58, 163
Maeder A., Lequeux J., 1982, A&A, 114, 409
Maeder A., Meynet G., 2000, ARA&A, 38, 143
Maíz Apellániz J., Walborn N. R., Morrell N. I., Niemela V. S., Nelan E. P., 2007, ApJ, 660, 1480
Malchenko S. L., Tarasov A. E., 2009, Astrophysics, 52, 235
Marchenko S. V., Moffat A. F. J., Koenigsberger G., 1994, ApJ, 422, 810
Marchenko S. V., Moffat A. F. J., Eenens P. R. J., 1998, PASP, 110, 1416
Marchenko S. V. et al., 2004, MNRAS, 353, 153
Marchenko S. V., Moffat A. F. J., Crowther P. A., 2010, ApJ, 724, L90
Marston A., Mauerhan J. C., Van Dyk S., Cohen M., Morris P., 2013, in Massive Stars: From Alpha to Omega, 167, Rhodes, Greece, preprint (arXiv:1309.1584)
Martín M. C., Cappa C. E., Testori J. C., 2007, Rev. Mex. Astron. Astrofis., 43, 243
Martins F., Plez B., 2006, A&A, 457, 637
Martins F., Schaerer D., Hillier D. J., 2005, A&A, 436, 1049
Martins F., Hillier D. J., Paumard T., Eisenhauer F., Ott T., Genzel R., 2008, A&A, 478, 219
Massey P., Conti P. S., 1983, ApJ, 273, 576
Massey P., Duffy A. S., 2001, ApJ, 550, 713
Massey P., DeGioia-Eastwood K., Waterhouse E., 2001, AJ, 121, 1050
Massey P., Olsen K. A. G., Parker J. W., 2003, PASP, 115, 1265
Massey P., Neugent K. F., Morrell N., Hillier D. J., 2014, ApJ, 788, 83
Mauerhan J. C., van Dyk S. D., Morris P. W., 2009, PASP, 121, 591
Mauerhan J. C., Muno M. P., Morris M. R., Stolovy S. R., Cotera A., 2010a, ApJ, 710, 706
Mauerhan J. C., Wachter S., Morris P. W., Van Dyk S. D., Hoard D. W., 2010b, ApJ, 724, L78
Mauerhan J. C., Cotera A., Dong H., Morris M. R., Wang Q. D., Stolovy S. R., Lang C., 2010c, ApJ, 725, 188
Mauerhan J. C., Van Dyk S. D., Morris P. W., 2011, AJ, 142, 40
Mel'Nik A. M., Dambis A. K., 2009, MNRAS, 400, 518
Melena N. W., Massey P., Morrell N. I., Zangari A. M., 2008, AJ, 135, 878
Messineo M., Davies B., Ivanov V. D., Figer D. F., Schuller F., Habing H. J., Menten K. M., Petr-Gotzens M. G., 2009, ApJ, 697, 701
Messineo M., Davies B., Figer D. F., Kudritzki R. P., Valenti E., Trombley C., Najarro F., Rich R. M., 2011, ApJ, 733, 41
Meynet G., Maeder A., 2005, A&A, 429, 581
Mikles V. J., Eikenberry S. S., Muno M. P., Bandyopadhyay R. M., Patel S., 2006, ApJ, 651, 408
Miszalski B., Crowther P. A., De Marco O., Köppen J., Moffat A. F. J., Acker A., Hillwig T. C., 2012, MNRAS, 423, 934
Moffat A. F. J., 1989, ApJ, 347, 373
Moffat A. F. J. Shara M. M., 1983, ApJ, 273, 544
Moffat A. F. J., Lamontagne R., Seggewiss W., 1982, A&A, 114, 135
Moffat A. F. J., Shara M. M., Potter M., 1991, AJ, 102, 642
Monnier J. D. et al., 2011, ApJ, 742, 1
Morris P. W., Brownsberger K. R., Conti P. S., Massey P., Vacca W. D., 1993, ApJ, 412, 324
Motch C. et al., 2010, A&A, 523, A92
Nakanishi H., Sofue Y., 2003, PASJ, 55, 191
Nakanishi H., Sofue Y., 2006, PASJ, 58, 847
Neugent K. F., Massey P., Morrell N., 2012, AJ, 144, 162
Nishiyama S., Tamura M., Hatano H., Kato D., Tanabé T., Sugitani K., Nagata T., 2009, ApJ, 696, 1407
Oskinova L. M., 2005, MNRAS, 361, 679
Paladini R., Davies R. D., De Zotti G., 2004, MNRAS, 347, 237
Parker Q. A. et al., 2005, MNRAS, 362, 689
Penny L. R., Gies D. R., 2009, ApJ, 700, 844
Pollock A. M. T., Haberl F., Corcoran M. F., 1995, in van der Hucht K. A., Williams P. M., eds, Proc. IAU Symp. 163, Wolf-Rayet Stars: Binaries, Colliding Winds, Evolution. Kluwer, Dordrecht, p. 512
Poveda A., Ruiz J., Allen C., 1967, Bol. Obs. Tonantzintla Tacubaya, 4, 86
Przybilla N., Butler K., Becker S. R., Kudritzki R. P., 2006, A&A, 445, 1099
Puls J., Vink J. S., Najarro F., 2008, A&AR, 16, 209
Rahman M., Moon D.-S., Matzner C. D., 2011, ApJ, 743, L28
Rauw G. et al., 2005, A&A, 432, 985
Rauw G., Manfroid J., Gosset E., Nazé Y., Sana H., De Becker M., Foellmi C., Moffat A. F. J., 2007, A&A, 463, 981
Rauw G., Sana H., Nazé Y., 2011, A&A, 535, A40
Reid M. J., Menten K. M., Zheng X. W., Brunthaler A., Xu Y., 2009, ApJ, 705, 1548
Reid M. J., McClintock J. E., Narayan R., Gou L., Remillard R. A., Orosz J. A., 2011, ApJ, 742, 83
Rieke G. H., Lebofsky M. J., 1985, ApJ, 288, 618
Rolleston W. R. J., Trundle C., Dufton P. L., 2002, A&A, 396, 53
Rolleston W. R. J., Venn K., Tolstoy E., Dufton P. L., 2003, A&A, 400, 21
Roman-Lopes A., 2011a, MNRAS, 410, 161
Roman-Lopes A., 2011b, ISRNA&A, 2011E, 8
Roman-Lopes A., 2012, MNRAS, 427, L65
Roman-Lopes A., 2013, MNRAS, 433, 712
Roman-Lopes A., Barba R. H., Morrell N. I., 2011, MNRAS, 416, 501
Rygl K. L. J. et al., 2012, A&A, 539, A79
Sana H., Gosset E., Rauw G., Sung H., Vreux J.-M., 2006, A&A, 454, 1047
Sander A., Hamann W.-R., Todt H., 2012, A&A, 540, A144
Schaerer D., Vacca W. D., 1998, ApJ, 497, 618

Schnurr O., Casoli J., Chené A.-N., Moffat A. F. J., St-Louis N., 2008, MNRAS, 389, L38
Schweickhardt J., Schmutz W., Stahl O., Szeifert Th., Wolf B., 1999, A&A, 347, 127
Shara M. M., Smith L. F., Potter M., Moffat A. F. J., 1991, AJ, 102, 716
Shara M. M., Moffat A. F. J., Smith L. F., Niemela V. S., Potter M., Lamontagne R., 1999, AJ, 118, 390
Shara M. M. et al., 2009, AJ, 138, 402
Shara M. M., Faherty J. K., Zurek D., Moffat A. F. J., Gerke J., Doyon R., Artigau E., Drissen L., 2012, AJ, 143, 149
Shetty R., Ostriker E. C., 2008, ApJ, 684, 978
Skrutskie M. F. et al., 2006, AJ, 131, 1163
Smith L. F., 1968, MNRAS, 141, 317
Smith N., 2006, ApJ, 644, 1151
Smith N., Tombleson R., 2015, MNRAS, 447, 602
Smith L. F., Shara M. M., Moffat A. F. J., 1990, ApJ, 358, 229
Smith L. F., Shara M. M., Moffat A. F. J., 1996, MNRAS, 281, 163
Smith J. D. T., Cushing M., Barletta A., McCarthy D., Kulesa C., Van Dyk S. D., 2012, AJ, 144, 166
Stead J. J., Hoare M. G., 2009, MNRAS, 400, 731
Stock D. J., Barlow M. J., 2010, MNRAS, 409, 1429
Todt H. et al., 2013, MNRAS, 430, 2302
Tovmassian H. M., Navarro S. G., Cardona O., 1996, AJ, 111, 306
Turner D. G., 1980, ApJ, 235, 146
Turner D. G., Rohanizadegan M., Berdnikov L. N., Pastukhova E. N., 2006, PASP, 118, 1533
Tuthill P. G., Monnier J. D., Lawrance N., Danchi W. C., Owocki S. P., Gayley K. G., 2008, ApJ, 675, 698
Underhill A. B., Hill G. M., 1994, ApJ, 432, 770
van der Hucht K. A., 2001, New Astron. Rev., 45, 135
van der Hucht K. A., 2006, A&A, 458, 453
van Leeuwen F., 2007, A&A, 474, 653
Varricatt W. P., Ashok N. M., 2006, MNRAS, 365, 127
Vázquez R. A., Baume G., 2001, A&A, 371, 908
Vazquez R. A., Will J.-M., Prado P., Feinstein A., 1995, A&AS, 111, 85
Vázquez R. A., Baume G. L., Feinstein C., Nuñez J. A., Vergne M. M., 2005, A&A, 430, 471
Wachter S., Mauerhan J. C., Van Dyk S. D., Hoard D. W., Kafka S., Morris P. W., 2010, AJ, 139, 2330
Wegner W., 2006, MNRAS, 371, 185
Williams P. M., van der Hucht K. A., Pollock A. M. T., Florkowski D. R., van der Woerd H., Wamsteker W. M., 1990a, MNRAS, 243, 662
Williams P. M., van der Hucht K. A., Sandell G., The P. S., 1990b, MNRAS, 244, 101
Williams P. M., van der Hucht K. A., Bouchet P., Spoelstra T. A. Th., Eenens P. R. J., Geballe T. R., Kidger M. R., Churchwell E., 1992, MNRAS, 258, 461
Williams P. M. et al., 2001, MNRAS, 324, 156
Williams P. M., Rauw G., van der Hucht K. A., 2009, MNRAS, 395, 2221
Wright E. L. et al., 2010, AJ, 140, 1868
Yusof N. et al., 2013, MNRAS, 433, 1114

APPENDIX A: RECENTLY DISCOVERED WR STARS

In Table A1 we provide identifications and coordinates of all 322 WR stars discovered between publication of the Annex (van der Hucht 2006) to the VIIth catalogue of WR stars (van der Hucht 2001) and 2014 March. Table A1 includes revised distances for stars for which high-quality near-IR photometry and a well-determined spectral type ($\pm$ 1) are available.

Following a request to the IAU Working Group for Massive Stars, a panel comprising P. A. Crowther, W.-R. Hamann, I. D. Howarth, K. A. van der Hucht, and G. Rauw came up with a set of proposals that was approved by the Working Group in 2012 December. Consequently, a revised nomenclature scheme has been introduced for Galactic WR stars as follows.

(i) All WR identifications up to the VIIth Catalogue (van der Hucht 2001) and Annex (van der Hucht 2006) remain unchanged since many are in widespread usage in the literature (e.g. WR 20 and WR 20a).

(ii) All subsequent discoveries are switched from alphabetical (WRXXa, b) to numerical (WRXX-1, −2) identification, sorted by

Table A1. WR stars discovered since the van der Hucht (2006) updated catalogue (up to 2014 March). Distances are indicated for the stars that feature in this study.

WR	Alias	RA (hh:mm:ss)	Dec. (±dd:mm:ss)	Ref.	Sp. type	Distance (kpc)
17−1	SMG09 668_4	10:16:26.226	−57:28:05.70	1	WN5b	5.4 ± 0.9
20−2	WR 20aa, SS215	10:23:23.49	−58:00:20.80	19	O2 If/WN6	–
20−1	MDM11 1	10:23:28.80	−57:46:29.4	5	WN7–8	–
20−3	WR 20c	10:25:02.60	−57:21:47.30	19	O2 If/WN6	–
42−1	WR 42e, SB04 #954	11:14:45.50	−61:15:00.1	21	O2 If/WN6	–
43−2	MTT 58	11:15:07.60	−61:16:54.8	22	O2 If/WN6	–
43−1	SMG09 740_21	11:16:03.536	−61:26:58.34	1	WN4b	6.9 ± 1.2
44−1	SMG09 740_16	11:19:42.96	−61:27:12.40	1	WCE	–
45−1	HDM07 1	11:42:37.66	−62:41:19.30	2	WN9–10h	–
45−2	SMG09 768_6	11:46:06.66	−62:47:12.70	1	WN5	–
...	...	...	...	...	...	...

(0) This work, (1) Shara et al. (2009), (2) Hadfield et al. (2007), (3) Mauerhan, van Dyk & Morris (2009), (4) Kurtev et al. (2007), (5) Mauerhan et al. (2011), (6) Davies et al. (2012b), (7) Roman-Lopes (2011b), (8) Roman-Lopes (2011a), (9) Wachter et al. (2010), (10) Shara et al. (2012), (11) Mauerhan et al. (2010a), (12) Mauerhan et al. (2010c), (13) Mauerhan et al. (2010b), (14) Liermann et al. (2009), (15) Messineo et al. (2009), (16) Gvaramadze et al. (2010), (17) Hanson et al. (2010), (18) Littlefield et al. (2012), (19) Roman-Lopes et al. (2011), (20) Motch et al. (2010), (21) Roman-Lopes (2012), (22) Roman-Lopes (2013), (23) Chené et al. (2013), (24) Rahman, Moon, Matzner (2011), (25) Anderson et al. (2011), (26) Marston et al. (2013), (27) Kanarek et al. (2014), (28) Davies et al. (2012a), (29) de La Fuente et al. (2013), (30) Borissova et al. (2012), (31) Mikles et al. (2006), (32) Hyodo et al. (2008), (33) Faherty et al. (2014), (34) Smith et al. (2012), (35) Corradi et al. (2010), (36) Gvaramadze et al. (2009), and (37) Burgemeister et al. (2013).

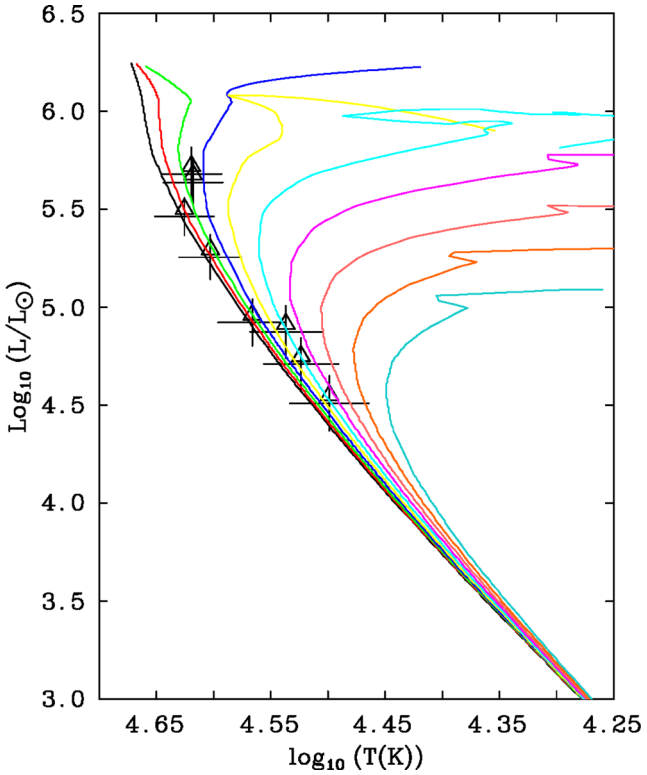

Figure B1. Hertzsprung-Russell diagram showing positions of the eight brightest (*V* band; Massey et al. 2001) O stars in the Pismis 24 open cluster (triangles). Stars are individually dereddened and shown at a distance modulus of 11.5, with $Z = 0.02$ isochrones (Lejeune & Schaerer 2001) for ages (from left to right) 6.00, 6.09, 6.19, 6.30, 6.40, 6.50, 6.59, 6.69, 6.80, and 6.90 Myr (left to right, solid lines).

year/month of discovery, in RA order if multiple discoveries arise from a single source. By way of example, three WR stars have been discovered since 2006 between the RA's of WR 20 and WR 21. The first, discovered by Mauerhan et al. (2011), is assigned WR 20−1, while two further discoveries from Roman-Lopes, Barba, & Morrell (2011) are assigned WR 20−2 and −3 (RA ordered).

(iii) Multiple WR stars identified within a single source are indicated with CAPITAL letters (e.g. WR 43a, b, c replaced with WR 43A, B, C).

(iv) The current Galactic WR census is maintained at http://pacrowther.staff.shef.ac.uk/WRcat/

APPENDIX B: WR STARS AND CLUSTERS WITH DISTANCE AMBIGUITY

B0.1 Pismis 24 and WR 93

The open cluster Pismis 24 (Pi 24) contains the WC7+O binary system WR 93, and has conflicting distance measurements in the literature, i.e. 2.56 ± 0.10 kpc (Massey, DeGioia-Eastwood & Waterhouse 2001) and 1.7 ± 0.2 kpc (Fang et al. 2012). In Fig. B1, we plot Lejeune & Schaerer (2001) isochrones along with the positions of the eight brightest O stars in Pi 24. We take photometry and spectral types for these O stars from Massey et al. (2001) except for Pi 24–1, which has since been resolved into two components, Pi 24–1 north-east (NE) and Pi 24–1 south-west (SW; Maíz Apellániz et al. 2007), with an optical/near ultraviolet $\Delta m \sim 0.1$. We adjust the Massey et al. photometry for Pi 24–1 to account for its binary nature, and adopt spectral types of O3.5If* and O4III(f+) for Pi 24–1 NE and Pi 24–1 SW, respectively (Maíz Apellániz et al. 2007). To calculate an extinction to each of the eight O stars, we evaluate the $E(B-V)$ colour excess assuming Martins & Plez (2006) intrinsic colours and an $R_V = 3.1$ extinction law. Finally, by taking O-star temperatures and bolometric corrections from Martins, Schaerer & Hillier (2005), we see that best agreement with the isochrones is found at a distance modulus of 11.5 ± 0.2, corresponding to $d = 2.00^{+0.19}_{-0.17}$ kpc.

B0.2 Westerlund 2

The distance to the young massive open cluster Westerlund 2 – probable host of the O3If*/WN6+O3If*/WN6 binary WR 20a (Rauw, Sana & Nazé 2011) and WR 20b (WN6ha) – remains controversial. The literature values range from 2.5 to 8 kpc, bringing the membership of the very luminous WR 20a into doubt. Rauw et al. (2007) used the light curve of WR 20a and the knowledge that both stars are of identical spectral type to derive a distance of 8.0 ± 1.0 kpc for this binary system. These authors also derive a distance to the Westerlund 2 cluster of 8.0 ± 1.4 kpc from spectro-photometry of cluster O stars and use this agreement as evidence for membership of WR 20a. However, these distances are derived on the assumption of an $R_V = 3.1$ extinction law, yielding an average $A_V = 4.68$ for the cluster. Carraro et al. (2012) have claimed an anomalous extinction law along this line of sight with an average $R_V = 3.8 \pm 0.2$. These authors use the spectra of Rauw et al. to obtain $A_V = 7.1 \pm 1.2$, corresponding to a much smaller distance of 3.02 ± 0.52 kpc. The membership of WR 20a as two ∼80 $M_\odot$ stars is unfeasible at such a small distance.

WR 20b shows no evidence of binarity in the spectroscopic and photometric monitoring of Rauw et al. (2007). The assumed intrinsic near-IR colour of WN6ha stars (Table 4) provides $A_{K_S} = 0.75 \pm 0.05$ ($A_V \sim 6.8$), favouring the higher extinction and lower distance estimate for Westerlund 2. Until the issue of the form of the extinction law to Westerlund 2 is settled, we consider neither WR 20a or WR 20b as members of the cluster. We include the stars of WR 20a in our calibration at the binary orbit-derived distance of 8.0 kpc.

B0.3 The Galactic Centre

The Arches and Quintuplet clusters are found at 11.6 and 13.1 arcmin from Sgr A*, respectively, which is itself surrounded by a cluster of massive stars. The distance to the GC (R_o), and these three clusters by association, has been the subject of considerable study. The first direct parallax measurement of a GC object – the star-forming region Sgr B2 – was presented by Reid et al. (2009) giving a distance of 7.9 ± 0.8 kpc; from kinematic arguments Sgr B2 is estimated to be 0.13 kpc nearer than the GC. The most recent determinations of R_o are summarized by Gillessen et al. (2013), and are converging on 8 kpc. Acknowledging the spread in measurements that still remains, we assume a distance of 8.0 ± 0.25kpc for these three clusters.

B0.4 The G305 complex

There are nine currently identified WR stars located within the boundary of the giant H II region G305.4+0.1, of which only four reside in the two central clusters Danks 1and2 (see fig. 16 of Mauerhan et al. 2011; Davies et al. 2012b). This is rather surprising, as one may expect to find these stars – as highly evolved descendants of massive progenitors – at the centre of these star clusters due to relaxation of their orbits. However, in the dense environment of a

cluster a massive star is more likely to encounter other massive stars or binaries, resulting in possible ejection. The apparent concentration of these five non-cluster WR stars in G305 around the younger Danks 1 cluster (Davies et al. 2012b) supports a dynamical ejection scenario.

Located only ∼2.3 arcmin from the Danks 1 cluster, WR 48 − 4 is the faintest WR star located within G305. Mauerhan et al. (2011) note that by assuming a WC7 spectral type and applying the K_S-band absolute magnitude-subtype calibrations of Crowther et al. (2006a), this star appears to be twice as distant as the two central clusters yet is reddened by a similar amount. As there is little evidence – other than the high IR-derived distance to WR48 − 4 – to suggest these nine WR stars are unassociated with G305, we include them in the calibration sample at the distance derived for the two central clusters.

APPENDIX C: SINGLE WR STAR EMISSION LINE STRENGTHS

In Table C1, we present average strengths for the most prominent lines in the spectra of each WR spectral type, gathered from

Table C1. Emission line strengths (equivalent widths, Å) in (apparently) single WR stars.

Spectral type	Star (WR#)	Equivalent width (Å)	Ref.	Average (Å)
He II 1.012 μm				
WN7	55	109.5	a, b	89
	82	75.9	b	
	84	134.6	b	
	120	70.8	c, d	
WN6	115	126	c, d	119
	85	112	a	
WN4–5	83	192.4	b	221
	54	236.2	b	
	61	243.8	b	
	149	234	a	
	129	200	a	
WN4b	1	377	e	412
	18	447	a	
WN5–6b	75	327	b	375
	110	423	a, d	
WN7b	77sc	280	f	
WC8	135	93	e	93
	57	121.7	b	
	60	111.1	b	
	118−4	80	g	
	119−2	93	g	
	53	61.7	a	
WC7	56	143.8	b	147
	64	145.8	b	
	90	162	b	
	124−3	138	g	
WC6	154	205	e	179
	107a	182	b	
	23	151	a	
WC4–5	111	218	e	225
	17	263	a	
	52	234	b	
	150	186	a	
He I 1.083 μm				
WN8	116	480	e	308
	130	200	e	
	16	245	d	

Table C1 – *continued*

Spectral type	Star (WR#)	Equivalent width (Å)	Ref.	Average (Å)
WN7	55	296	b	291
	82	309	b	
	84	267	b	
WN6	115	170	d	170
WN4–5	83	95	b	114
	54	106	b	
	61	142	b	
WN7b	77sc	930	f	930
WN5–6b	75	661	b	712
	110	763	d	
WN4b	1	452	e	
WC8	57	221	b	412
	60	353	b	
	118−4	537	g	
	119−2	600	g	
	135	344	e	
WC7	56	221	b	227
	64	171	b	
	90	301	b	
	124−3	215	g	
WC6	5	276	e	232
	107a	200	b	
	154	220	e	
WC4–5	52	149	b	169
	111	189	e	
He I–II 2.164 μm				
WN8–9	16	75	d	73
	105	63	d	
	116	106	e	
	130	46	e	
WN7	55	33	b	43
	120	52	d	
WN6	24	34	d	35
	115	36	d	
WN4–5	129	50	h	53
	149	55	h	
WN7b	77sc	85	f	
WN6b	75	74	b	
WN4b	1	54	e	
He II 2.189 μm				
WN7	120	39	d	35
	55	31	b	
WN6	115	58	d	42
	24	25	d	
WN4–5	129	110	h	105
	149	99	h	
C IV 2.071-2.084 μm				
WC8	48−2	581	b	466
	77g	430	f	
	118−4	303	g	
	119−2	433	g	
	135	583	e	
WC7	67−2	783	i	937
	90	825	b	
	124−3	1202	g	
WC6	5	1339	e	1530
	48−4	1862	b	
	154	1388	e	
WC4–5	52	1169	b	1391
	111	1613	e	
C III 2.104−2.115 μm				
WC8	48−2	220	b	209
	77g	198	f	

Table C1 – *continued*

Spectral type	Star (WR#)	Equivalent width (Å)	ref	Average (Å)
	118−4	173	g	
	119−2	260	g	
	135	192	e	
WC7	67−2	234	i	293
	90	224	b	
	124−3	422	g	
WC6	5	228	e	301
	48−4	385	b	
	154	289	e	
WC4–5	52	277	b	290
	111	302	e	

(a) Conti, Massey & Vreux (1990), (b) P. A. Crowther (private communication), (c) Howarth & Schmutz (1992), (d) Crowther & Smith (1996), (e) W. D. Vacca (private communication), (f) Crowther et al. (2006a), (g) Mauerhan et al. (2011), (h) Figer, McLean & Najarro (1997), and (i) Roman-Lopes (2011a).

published spectra of single WR stars. We use these values to calculate J and K_S-band continuum flux ratios in cases where WR emission lines are diluted by an unknown companion. An uncertainty of 0.1 dex is assumed on each averaged equivalent width, in accordance with the majority of studies from which individual measurements are taken.

APPENDIX D: A VOLUME-LIMITED SAMPLE OF WR STARS

We present a volume-limited ($d < 3$ kpc) sample of Galactic WR stars in Table D1, in which distances are either from this work, or are derived by adopting M_v (by subtype) and A_v from van der Hucht (2001).

Table D1. Closest ($d < 3$kpc) WR stars listed in ascending heliocentric distance. In the fourth column we class each system as WR-dominated ($m_K^{\rm WR} - m_K^{\rm sys} > 0.4$; WR), companion dominated (C), or dust producing (D). References are given for spectral types of stars not appearing in Tables 1– 3 or 8 (online).

WR#	Spectral type	Distance (kpc)	Class
11	WC8+O7.5III	0.34 ± 0.08	C
147	WN8(h)+OB	0.73 ± 0.12	WR
94	WN5	0.78 ± 0.12	WR
90	WC7	1.15 ± 0.19	WR
136	WN6b(h)	1.3 ± 0.2	WR
137	WC7+O9	1.3 ± 0.2	D
139	WN5+O6III–V	1.3 ± 0.2	C
141	WN5+O5III–V	1.3 ± 0.2	C
143	WC4+Be	1.33 ± 0.33	C
138	WN5+OB	1.38 ± 0.26	C
144	WC4	1.40 ± 0.08	WR
52	WC4	1.54 ± 0.23	WR
110	WN5b	1.55 ± 0.24	WR
9	WC5+O7⋆	1.57 ± 0.58⋆	C
15	WC6	1.57 ± 0.49	WR
81	WC9	1.64 ± 0.34	WR

Table D1 – *continued*

WR#	Spectral type	Distance (kpc)	Class
78	WN7	1.64 ± 0.03	WR
79	WC7+O5–8V	1.64 ± 0.03	C
79a	WN9ha	1.64 ± 0.03	WR
140	WC7pd+O5fcIII–I[1]	1.67 ± 0.03[2]	D
142−1	WN6	1.70 ± 0.34	WR
6	WN4b	1.80 ± 0.27	WR
121	WC9d⋆	1.8 ± 0.4⋆	D
142a	WC7	1.83 ± 0.31	WR
105	WN9	1.9 ± 0.2	WR
111	WC5	1.9 ± 0.2	WR
134	WN6b	1.9 ± 0.2	WR
135	WC8	1.9 ± 0.2	WR
86	WC7+B0III	1.97 ± 0.47	WR
113	WC8d+O8–9⋆	2.0 ± 0.2	D
14	WC7	2.0 ± 0.1	WR
93	WC7+O7–9	2.0 ± 0.2	WR
114	WC5	2.05 ± 0.09	WR
115	WN6	2.05 ± 0.09	WR
70	WC9vd+B0I⋆	2.1 ± 0.4⋆	D
47	WN6+O5.5	2.13 ± 0.44	WR
133	WN5+O9I	2.14 ± 0.07	C
70−5	WC9	2.17 ± 0.45	WR
48	WC6+O6–7V[3]... +O9.5/B0Iab⋆	< 2.3⋆	C
1	WN4b	2.3 ± 0.5	WR
103	WC9d⋆	2.3 ± 0.5⋆	D
59	WC9d⋆	2.3 ± 0.5⋆	D
2	WN2b+B[4]	2.4 ± 0.8	WR
106	WC9d⋆	2.4 ± 0.6⋆	D
19a	WN7	2.41 ± 0.47	WR
101	WC8	2.46 ± 0.43	WR
40	WN8h	2.48 ± 0.41	WR
95	WC9d⋆	2.5 ± 0.5	D
60	WC8	2.55 ± 0.45	WR
155	WN6+O9II–Ib	2.56 ± 0.56	WR
117−1	WN7	2.59 ± 0.50	WR
18	WN4b	2.6 ± 0.2	WR
22	WN7ha+O9III–V	2.6 ± 0.2	WR
23	WC6	2.6 ± 0.2	WR
24	WN6ha	2.6 ± 0.2	WR
25	O2.5If*/WN6[5]+OB	2.6 ± 0.2	C
104	WC9d+B0.5V⋆	2.6 ± 0.7	D
88	WC9	2.67 ± 0.54	WR
4	WC5	2.69 ± 0.49	WR
5	WC6	2.69 ± 0.84	WR
72−1	WC9	2.73 ± 0.56	WR
16	WN8h	2.77 ± 0.46	WR
85	WN6	2.8 ± 1.1	WR
111−3	WC8	2.80 ± 0.49	WR
69	WC9d+OB⋆	2.8 ± 0.6⋆	D
75b	WC9	2.82 ± 0.58	WR
124−8	WN6	2.84 ± 0.56	WR
113−1	WN7	2.88 ± 0.56	WR
151	WN4+O5V	2.93 ± 0.65	WR
42	WC7+O7V	2.96 ± 0.53	C
57	WC8	2.97 ± 0.52	WR
75a	WC9	2.98 ± 0.60	WR

⋆ van der Hucht (2001),
(1) Fahed et al. (2011),
(2) Monnier et al. (2011),
(3) Hill, Moffat & St-Louis (2002),
(4) Chené et al. (2014), and
(5) Crowther & Walborn (2011).

SUPPORTING INFORMATION

Additional Supporting Information may be found in the online version of this article:

Table 8. Calculated spatial locations of the 228 'field' WR stars showing no conclusive evidence for an IR-bright companion, to which our calibrated absolute magnitudes have been assigned.
Table A1. WR stars discovered since the van der Hucht (2006) updated catalogue (up to 2014 March).

(http://mnras.oxfordjournals.org/lookup/suppl/doi:10.1093/mnras/stu2525/-/DC1).

Please note: Oxford University Press is not responsible for the content or functionality of any supporting materials supplied by the authors. Any queries (other than missing material) should be directed to the corresponding author for the paper.

This paper has been typeset from a TEX/LATEX file prepared by the author.